ORNL/TM-6632
ENDF-290

ornl

OAK
RIDGE
NATIONAL
LABORATORY

UNION
CARBIDE

Preliminary Study of Pseudorandom Binary Sequence Pulsing of ORELA

Nancy M. Larson
David K. Olsen

OPERATED BY
UNION CARBIDE CORPORATION
FOR THE UNITED STATES
DEPARTMENT OF ENERGY

Printed in the United States of America. Available from
National Technical Information Service
U.S. Department of Commerce
5285 Port Royal Road, Springfield, Virginia 22161
NTIS price codes—Printed Copy: A05; Microfiche A01

ORNL/TM-6632
ENDF-290
Dist. Category UC-79d

Contract No. W-7405-eng-26

Engineering Physics Division

PRELIMINARY STUDY OF PSEUDORANDOM BINARY SEQUENCE PULSING OF ORELA

Nancy M. Larson* and David K. Olsen

Manuscript Completed - January 9, 1980

Date Published - March 1980

*Computer Sciences Division

Prepared by the
OAK RIDGE NATIONAL LABORATORY
Oak Ridge, Tennessee 37830
operated by
UNION CARBIDE CORPORATION
for the
DEPARTMENT OF ENERGY

CONTENTS

LIST OF FIGURES

ABSTRACT

It has been suggested that pseudorandom binary sequence (PRBS) pulsing might enhance the performance of the Oak Ridge Electron Linear Accelerator (ORELA) for neutron-induced, time-of-flight (TOF) cross-section measurements. In this technical memorandum, equations are developed for expected count rates, statistical variances, and backgrounds for a pulsing scheme in which a PRBS is superimposed on the periodic equal-intensity ORELA bursts. Introduction of the PRBS modification permits neutrons of different energies originating from different bursts to reach the detector simultaneously, and the signal corresponding to a unique flight time to be extracted mathematically. Relative advantages and disadvantages of measurements from conventional and PRBS pulsing modes are discussed in terms of counting statistics and backgrounds. Computer models of TOF spectra are generated for both pulsing modes, using as examples a 20-meter ^{233}U fission-chamber measurement and a 155-meter ^{238}U sample-in transmission measurement. Detailed comparisons of PRBS vs conventional results are presented. This study indicates that although PRBS pulsing could enhance ORELA performance for selected measurements, for general ORELA operation the disadvantages from PRBS pulsing probably outweigh the advantages.

I. INTRODUCTION

Although originally suggested for neutron time-of-flight (TOF) measurements with Van de Graaff accelerators,[1] pseudorandom binary sequence (PRBS) pulsing techniques have been applied only to TOF measurements with neutron fluxes from research reactors.[2] With these "white source" beams, continuous in time, PRBS techniques allow higher statistical accuracy and lower backgrounds than the conventional TOF method for some types of measurements.

The suggestion has been made that similar techniques involving PRBS pulsing might prove useful on the Oak Ridge Electron Linear Accelerator (ORELA). At present many low energy experiments require low pulse repetition rates; the resulting low power output makes it impractical for other types of experiments to be performed concurrently. Introduction of a PRBS pulsing mode at ORELA would permit higher repetition rates for low energy experiments, thus increasing the overall utility of ORELA. This technical memorandum describes an initial study of the implications of PRBS pulsing on ORELA.

The basic principle involved is simple. In order that events from successive pulses do not overlap in time, the neutron pulse rate of conventional TOF measurements must be small enough that the time between pulses is greater than the longest flight time. This pulse rate limitation can be removed by modulating the flux on and off according to a PRBS. With the flux so modulated, a TOF spectrum is measured with events from successive pulses overlapping in time; and the measured spectrum is cross correlated with the PRBS of the incident neutron flux, giving

the desired conventional TOF spectrum. Flux utilization can be increased because PRBS pulsing allows a higher pulse rate and hence more neutrons to be utilized. The background component which is uncorrelated in either time or intensity with the incident flux is effectively reduced because, although its absolute magnitude remains unchanged, this background is distributed among overlapping foregrounds. However, there may be no reduction of statistical variances because the counting statistics of events overlapping in time are mixed.

Some PRBS advantages for measurements with reactors are not directly transferable to ORELA. For a given pulse width, neutron bursts from ORELA already contain the maximum flux which can be produced; thus there is no intensity advantage for those measurements which employ the maximum pulse rate and are not significantly affected by time overlap filters. In addition, for most measurements the flux-uncorrelated background is negligible with respect to the flux-correlated background. However, for many measurements the problem of time overlap from successive pulses is severe and is presently solved by pulsing ORELA at a smaller than maximum rate and/or employing Cd or B beam filter to remove the flux at low energies and hence long times. Some measurements are normalized at thermal energies where the cross sections are well known; thermal normalization at 20, 40, and 150 meters requires 25, 13, and 3 pulses per second, respectively. Measurements with small or radioactive samples can have a large flux-uncorrelated background. Because these measurements with significant time-overlap and uncorrelated-background problems utilize a significant fraction of the ORELA running time, a study of PRBS pulsing for such measurements is warranted.

This study begins with a detailed theoretical investigation of the application of PRBS pulsing at ORELA. General formulae representing the effect of PRBS on counting statistics are developed; the specific effects are discussed for prototype spectra (e.g. flat or sparse). The various types of backgrounds encountered in ORELA experiments are considered individually, and conclusions are drawn regarding the PRBS treatment of each type. Earlier results by Hossfeld and Amadori[3] on application of PRBS to reactors and by Larson, Crosmun, and Talmi[4] on application of PRBS to optical spectrometers, while not directly transferable to ORELA, have contributed to our understanding of this problem.

The theoretical study is augmented with computer models of two realistically measured spectra at different flight path lengths. ENDF/B-IV evaluated cross sections[5] are used for a 20-meter ^{233}U capture experiment. The entire experimental neutron range from .00137 eV to 3.7 MeV is simulated with ORELA pulsed both in the conventional mode and in the PRBS mode. No backgrounds are considered; the ratio of relative statistical errors is evaluated to determine the merit of PRBS pulsing.

The second experiment to be modeled is a simplified version of a 155-meter ^{238}U transmission experiment[6] for which we have assumed typical resonances at seven decimal energies from 0.1 eV to 100 keV. Expected foreground and background are calculated in the neighborhood of the resonances for ORELA operated in three different modes: PRBS mode, conventional mode with time-overlap filter, and conventional mode at a low repetition rate with no filter. Realistic backgrounds as understood by the experimenters[6] are employed.

A summary of PRBS mathematical properties is given in Section II of this report. Formulae describing PRBS application at ORELA are developed in Section III, and the computer simulations are described in Section IV. Summary, conclusions, and recommendations for further work are presented in Section V. Three appendices complete this report: the first generalizes the equations from Section III, the second proves results from Section II, and the third describes other possible uses for PRBS at ORELA.

II. SUMMARY OF PRBS MATHEMATICS

A pseudorandom binary sequence (PRBS) of period N is an ordered set of N integers, m of which are 1 and N-m of which are 0, satisfying certain mathematical properties. The duty cycle c is approximately that fraction of the integers which are 1's; for c = 1 all the integers are 1 and for c = 0 only one integer is 1. In Appendix A we show that the most useful value of c for ORELA applications is c = 1/2 for which m = (N+1)/2. In the text of this report, equations are given only for c = 1/2, with the corresponding equations for arbitrary c presented in Appendix A.

Let a_i represent the i^{th} member of a PRBS, where $0 \leq i < N$. If the subscript on a PRBS member falls outside the specified range, a periodic extension is made of the sequence; e.g., a_{2N+5} is given the value a_5. An example of a PRBS of period N = 3 is $\{a_0, a_1, a_2\} = \{0, 1, 1\}$, for which m = 2 and c = 1/2.

For sequence $\{a_i\}$ of period N to be a PRBS of duty cycle 1/2, its autocorrelation function C_{jk} must obey the equation

$$C_{jk} = \sum_{i=0}^{N-1} a_{i+j}\, a_{i+k} = \frac{N+1}{4}(\delta_{jk}+1) \quad . \tag{1}$$

That is, C_{jk} has the value (N+1)/2 if j = k and (N+1)/4 if $j \neq k$. Existence and generation of these sequences are discussed in Refs. 7 and 8. In particular, C = 1/2 sequences are known to exist for $N = 2^n-1$, where n is any integer ≥ 2.

The sequence $\{a_i^*\}$ may be defined by $a_i^* = 2a_i-1$, and the correlation of this sequence with $\{a_i\}$ is, using Eq. (1),

$$\frac{2}{N+1} \sum_{i=0}^{N-1} a_{i+j}\, a^*_{i+k} = \delta_{jk} \cdot \tag{2}$$

Because this correlation is a delta function, we hereafter refer to $\{a^*_i\}$ as the inverse sequence of $\{a_i\}$. Specifically, if a_i has the value 1 then a^*_i has the value 1, and if a_i is 0 then a^*_i is -1. For the N = 3 example the inverse sequence is {-1, 1, 1}.

The development of equations describing the application of PRBS to ORELA, described in Section III, is based entirely on Eqs. (1) and (2) and other PRBS properties derived from those equations. Elaborate mathematical derivations of those properties are reserved for Appendix B; important results are summarized here for easy reference.

The summation over all terms in the inverse sequence $\{a^*_i\}$ gives

$$\sum_{i=0}^{N-1} a^*_i = 1 \; ; \tag{3}$$

for the N = 3 example $a^*_0 + a^*_1 + a^*_2 = -1 + 1 + 1 = 1$. The sum of the squares of those terms is

$$\sum_{i=0}^{N-1} (a^*_i)^2 = N \; ; \tag{4}$$

for the example $(-1)^2 + (1)^2 + (1)^2 = 3$. The sum of the squares of those terms multiplied by a_{i+j} is

$$\sum_{i=0}^{N-1} a_{i+j}(a^*_i)^2 = (N+1)/2 \; ; \tag{5}$$

for the example $0\cdot(-1)^2 + 1\cdot(1)^2 + 1\cdot(1)^2 = 2$.

III. MATHEMATICAL DESCRIPTION OF CONVENTIONAL AND PRBS ORELA MODES

In this section a mathematical description of conventional and PRBS modes is presented. Notation is defined such that any given symbol will represent the same quantity in conventional and PRBS modes; in those cases where the value of the quantity varies between the two modes, the symbol is primed in the conventional mode.

A. Treatment Ignoring Backgrounds and Other Complicating Factors

In this subsection the basic equations governing PRBS application at ORELA are derived without regard to background effects, which are described in the following subsection. Conventional vs PRBS modes are compared on the basis of counting statistics alone. Channel widths are assumed to be of equal time duration; the complication of unequal channel widths is discussed in the last subsection.

1. Operation of ORELA under conventional mode

In the conventional pulsing mode presently used at ORELA, the flight-path length, beam filters, and ORELA repetition rate must be arranged so that each detector time channel records events for a unique TOF duration. A schematic of this situation is shown in Fig. 1, where τ represents the burst width, T_b' the time between bursts, θ the channel width, and T_s the time span during which all neutrons reach the detector. That is, T_b' is the reciprocal of the repetition rate, and T_s is the TOF difference between the slowest and fastest neutrons.

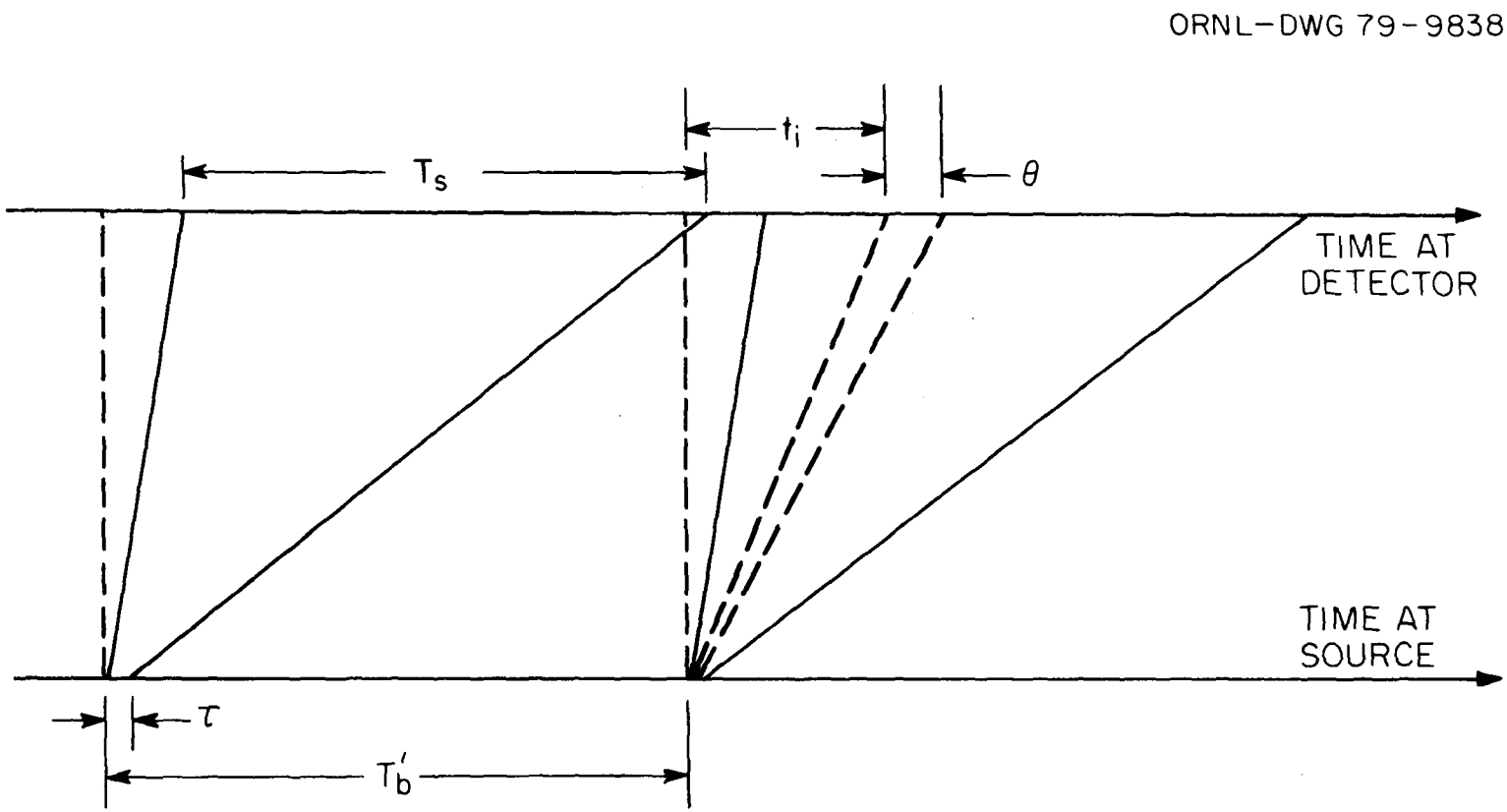

Fig. 1. Time sequence for neutron production and detection using the conventional ORELA pulsing modes. $1/T_b'$ neutron pulses per second of width τ spread in time according to velocity as they traverse the distance from source to detector. The time between the slowest and fastest neutron $T_s \leq T_b'$ to prevent frame overlap.

For channel i the detector counts S_i events per burst, whose neutron flight time from source to detector is t_i. If the total time for the experiment is T, there are $\ell' = T/T_b'$ bursts, so that $\ell' S_i$ events are counted. Since the counting statistics are described by a Poisson distribution, the statistical error associated with the detection of $\ell' S_i$ events is $\sqrt{\ell' S_i}$, giving a relative statistical error of $1/\sqrt{\ell' S_i}$ for each channel i.

In the conventional mode the time between bursts T_b' must be greater than the flight time T_s. Otherwise slow neutrons from previous bursts will arrive at the detector simultaneously with fast neutrons from the current burst, and be indistinguishable from them; this phenomenon is known as frame overlap. For measurements employing only fast neutrons the requirement $T_b' > T_s$ is easily met. For measurements employing slow neutrons this requirement can be met only by pulsing ORELA at a slower than maximum rate or by using beam filters to remove low energy neutrons. Both of these methods for preventing frame overlap greatly reduce the usable flux.

2. Operation of ORELA under PRBS mode

In the PRBS pulsing mode, the detector time channels are not required to record events for a single TOF channel. Rather, linear combinations of TOF channels are recorded in a detector-time channel, and the result is unfolded mathematically to determine the true number of events and their standard deviation for each TOF channel. A schematic of this situation is shown in Fig. 2. Again τ represents burst width, T_b the time between ORELA bursts, and T_s the TOF difference between the fastest and slowest neutrons. Although Fig. 2 shows equally spaced bursts, in fact the pattern of bursts is modified in a pseudorandom manner. That is,

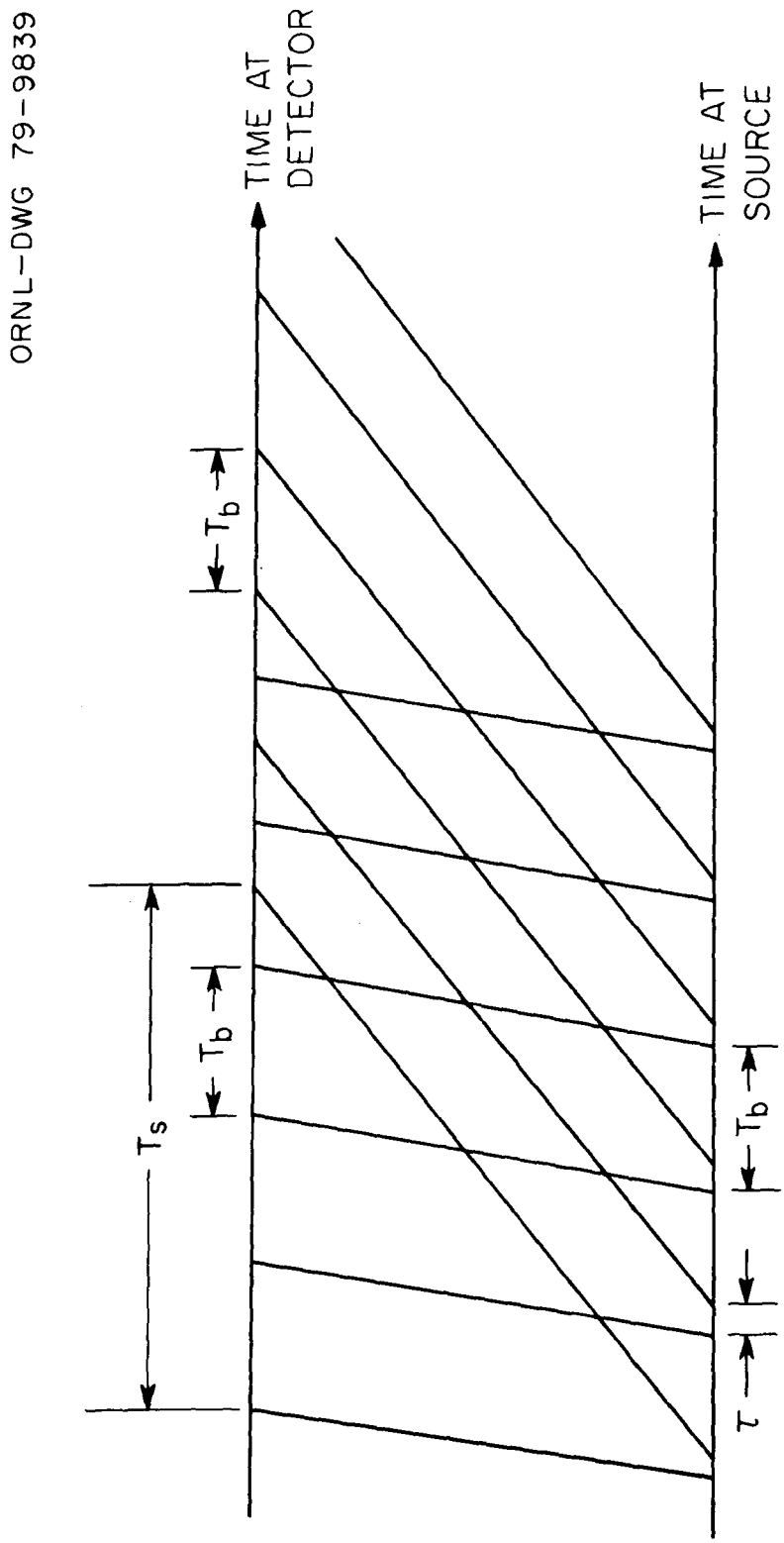

Fig. 2. Time sequence for neutron production and detection using PRBS pulsing for ORELA. Using a PRBS of length N allows a conventional TOF spectrum S to be unfolded from the detector spectrum Z produced from frame-overlapped neutrons. $T_s \leq NT_b$.

superimposed on the source is a repeating PRBS which removes approximately half the bursts.

Let N_b represent the number of detector-time channels of width θ spanning the time between bursts, so that $T_b = N_b\,\theta$. Similarly N_s represents the number of TOF channels between the fastest and slowest neutrons, so that $T_s = N_s\,\theta$. In order to successfully unfold all overlapping signals, it is necessary that the period of the PRBS be sufficiently long to cover the entire flight-time span between fastest and slowest neutrons. Since the PRBS will repeat itself after time $NT_b = NN_b\theta$, a necessary condition for successful operation in the PRBS pulsing mode is $NT_b > T_s$, or $NN_b > N_s$.

The detector system measures NN_b quantities $Z_k^{(n)}$, where k labels the detector time channel between bursts ($0 \leq k < N_b$) and n labels the particular burst in the PRBS ($0 \leq n < N$). The $Z_k^{(n)}$ are sums over all signals reaching the detector simultaneously. That is,

$$Z_k^{(n)} = \sum_{j=0}^{N-1} \ell S_{k+jN_b}\, a_{n-j} \quad , \text{ for } 0 \leq k < N_b \ , \ 0 \leq n < N \ , \tag{6}$$

where S_{k+jN_b} is the number of events per burst from neutrons whose TOF from source to detector is $t_{k+jN_b} = (k+jN_b)\,\theta$, and ℓ is the number of complete cycles through the PRBS. For total time T, ℓ is equal to $\frac{T}{T_b N}$. The PRBS element a_{n-j} represents the condition of the source for the $(n-j)^{th}$ burst; $a_{n-j} = 0$ indicates that the burst was absent, $a_{n-j} = 1$ indicates the burst was present.

To obtain the required signals, both sides of Eq. (6) are multiplied by the inverse sequence and summed over the sequence elements (i.e., over n), giving

$$\ell S_{k+jN_b} = \frac{2}{N+1} \sum_{n=0}^{N-1} Z_k^{(n)} \; a^*_{n-j} \; . \tag{7}$$

In reality, of course, no multiplication is involved, since the a*'s have predetermined values of either +1 or -1. Multiplication by 2/(N+1) may be delayed until the measurement is completed. It is important to note that the quantity S_{k+jN_b} on the right side of Eq. (6) from normal pulsing is identical to the quantity S_{k+jN_b} on the left side of Eq. (7) from the PRBS pulsing. It is the standard deviation of S_{k+jN_b} with respect to S_{k+jN_b} which is the quantity of interest and which differs for the two pulsing modes.

In the PRBS mode, the statistical error is no longer given by $\sqrt{\ell S_{k+jN_b}}$, since the Poisson statistics from counting apply not to the TOF events after inversion but to the events measured by the detector. That is, it is the $Z_k^{(n)}$ distribution which is Poisson. It is shown in Appendix A that the variance is given by

$$\mathrm{Var}(\ell S_{k+jN_b}) = (\frac{2}{N+1})^2 \sum_{n=0}^{N-1} (a^*_{n-j})^2 \; \mathrm{Var}[Z_k^{(n)}] \; , \tag{8}$$

or, since $a^*_{n-j} = \pm 1$,

$$\mathrm{Var}(\ell S_{k+jN_b}) = (\frac{2}{N+1})^2 \sum_{n=0}^{N-1} Z_k^{(n)} \; . \tag{9}$$

The variance of S_{k+jN_b} may also be written in terms of $S_{k+j^\circ N_b}$ as

$$\mathrm{Var}(\ell S_{k+jN_b}) = (\frac{2}{N+1})^2 \sum_{n=0}^{N-1} \sum_{j^\circ=0}^{N-1} \ell S_{k+j^\circ N_b} \; a_{n-j^\circ} \tag{10}$$

by substituting Eq. (6) for $Z_k^{(n)}$ in Eq. (9). After performing the sum over n we are left with

$$\mathrm{Var}(\ell S_{k+jN_b}) = \frac{2}{N+1} \sum_{j'=0}^{N-1} \ell S_{k+j'N_b} \quad . \tag{11}$$

This equation indicates that the total variance from all counts reaching the detector simultaneously is split equally among the contributing signals. The relative statistical error (RSE) for TOF channel $k+jN_b$ is then

$$\mathrm{RSE} = \frac{1}{\ell S_{k+jN_b}} \sqrt{\frac{2}{N+1} \sum_{j'=0}^{N-1} \ell S_{k+j'N_b}} \quad . \tag{12}$$

Thus a TOF channel with a high number of counts will have a relatively low RSE, and a TOF channel with a low number of counts will have a relatively high RSE.

3. Comparison of conventional mode vs PRBS mode

In the absence of background and other complicating factors, results for the two pulsing modes may be compared by considering their respective relative statistical errors. We assume that the total times allowed for the two measurements are equal, and that the pulse intensity and detector response are independent of pulsing mode or repetition rate.

For specific experimental arrangements the relative statistical error for the two modes can be generated and compared directly. Such comparisons are complicated and will be described in detail later. For illustration, consider the simplified case of equal channel widths and no time overlap filters. In this case the RSE for TOF channel $i = k+jN_b$ in the PRBS mode is

$$RSE_{k+jN_b} = \frac{\sqrt{\frac{2}{N+1}\frac{NT_b}{T}\sum_{j=0}^{N-1} S_{k+j\cdot N_b}}}{S_{k+jN_b}} \tag{13}$$

and, in the conventional mode

$$RSE'_i = \sqrt{\frac{T'_b}{T\,S_i}} \quad . \tag{14}$$

The ratio of these two RSE's is a figure of merit for the PRBS. Define the ratio $R_i = RSE_i/RSE'_i$; if R is greater than unity, the conventional mode is superior and if R is less than unity, the PRBS mode is superior. Evaluating R_i, for $i = k+jN_b$, one obtains,

$$R_{k+jN_b} = \left[\frac{2}{N+1}\frac{NT_b}{T'_b}\frac{\sum_{j=0}^{N-1} S_{k+j\cdot N_b}}{S_{k+jN_b}}\right]^{1/2} \quad . \tag{15}$$

It is necessary to resort to specific examples to evaluate this figure of merit. However, insight can be gained by considering the two following extreme examples assuming $NT_b/T'_b \simeq 1$; that is, a measurement using conventional pulsing is compared with an identical measurement using PRBS pulsing in which a PRBS of N bursts has been inserted between the conventional pulses.

(1) One of the N overlapping TOF channels has many counts, whereas the other TOF channels have very few counts. For convenience assume $S_k >> S_{k+jN_b}$ for $j \neq 0$. Then

$$R_k \approx \sqrt{2/(N+1)} < 1 \tag{16}$$

which implies that the PRBS mode would give smaller statistical errors over a peak. However, for the overlapping TOF channels with few counts

$$R_{k+jN_b} \simeq \left[\frac{2\,S_k}{(N+1)S_{k+jN_b}}\right]^{1/2} . \tag{17}$$

Whether this ratio is greater or less than unity depends on the relative values of N and the peak-to-valley ratio. For a TOF channel with relatively few counts, the conventional method does better.

(2) If the spectrum is completely flat, that is, if $S_{k+jN_b} \cong S$ for all TOF channels, then

$$R_{k+jN_b} \simeq \sqrt{2} \tag{18}$$

so that the conventional mode is superior on average, independent of N.

B. Treatment Including Backgrounds

1. Beam-uncorrelated time-independent background

Let d represent the total number of time-independent or beam-uncorrelated background events per burst counted by the detector in channel i of width θ. In the conventional mode the measured events in channel i are

$$O_i' = \ell'(S_i + d) \tag{19}$$

where ℓ' is exactly the number of bursts for the conventional mode measurement.

In the PRBS mode the uncorrelated background counted in a detector channel of width θ is also d. Each detector channel contains this background, so that

$$Z_k^{(n)} = \ell d + \sum_{j=0}^{N-1} \ell S_{k+jN_b} \, a_{n-j} \, . \tag{20}$$

Applying the inverse sequence {a*}, one obtains

$$\ell d \, \frac{2}{N+1} + \ell S_{k+jN_b} = \frac{2}{N+1} \sum_{n=0}^{N-1} Z_k^{(n)} \, a^*_{n-j} \, , \tag{21}$$

so that the measured events in TOF channel i of width θ is

$$O_i = \ell d \, \frac{2}{N+1} + \ell S_i \, . \tag{22}$$

The variance for this signal is shown in Appendix A to be

$$\mathrm{Var}\left(\ell d \, \frac{2}{N+1} + \ell S_{k+jN_b}\right) = \frac{4N}{(N+1)^2} \, \ell d + \frac{2}{N+1} \sum_{j^\circ=0}^{N-1} \ell S_{k+j^\circ N_b} \, . \tag{23}$$

In addition to the relative statistical error, the ratio of foreground to background should be a valid test of the merit of PRBS pulsing. For the conventional mode this ratio is S_i/d and for the PRBS mode this ratio is $S_i(\frac{N+1}{2})/d$, a factor of (N+1)/2 greater than for the conventional mode. This effective reduction in the magnitude of the uncorrelated background accounts for the great utility of PRBS in reactor TOF experiments. For most ORELA applications, however, uncorrelated background is not a significant contribution to the total count rate.

2. Beam-correlated background: Simple function

Let H(t) represent an ORELA target-produced background which arrives at the detector with a time dependence independent of the signal of interest and a magnitude proportional to the flux produced at the ORELA target. An example of this would be the background caused by hydrogen capture gamma rays produced in the moderating water of the target. These gamma rays emanate from the target with a half-life of about 17.5 μsec following the electron burst. Other examples are the high energy γ-rays which emanate immediately from the target, "gamma flash", and a room-return background treated as a smooth function of energy.

In the conventional mode for channel i the measured events O_i' are given by the sum of the signal S_i and the background H_i

$$O_i' = \ell'(S_i + H_i) \ . \tag{24}$$

Likewise, in the PRBS mode the detector records signal plus background

$$Z_k^{(n)} = \ell \sum_{j=0}^{N-1} \left(S_{k+jN_b} + H_{k+jN_b} \right) a_{n-j} \ . \tag{25}$$

This equation can be inverted to yield

$$O_i = \ell(S_i + H_i) \tag{26}$$

for the observed number of counts per TOF channel. Since this background scales in the same manner as the signal, we find mathematically that the effect of this background is the same in the PRBS mode as in the conventional mode.

However, caution must be observed. If the effect of the gamma flash is to overload the detector, this overload problem will be significantly more severe in the PRBS mode. In the conventional mode information will be lost for only a few channels which usually correspond to very high neutron energies. However, in the PRBS mode information will be lost for all TOF channels which overlap the gamma flash. Possibly this problem could be overcome by running two or more separate PRBS-mode measurements in which the time between pulses is varied slightly to obtain the entire spectrum.

3. Beam-correlated background: Folding function

Usually with ORELA measurements the most difficult background to subtract is the so-called "room return" or "fitted" background, which is produced by beam neutrons scattering from the collimators, air, sample, and detector apparatus. These neutrons return to the detector at later times to be counted as valid events. This background can be treated as a smooth function of energy as discussed above or by using a folding procedure as discussed below.

Let F_i represent this "fitted" background in channel i. In the conventional mode F_i may be treated as a linear sum over fractions of the signals reaching the detector at earlier times; mathematically,

$$F_i = \sum_{q<i} S_q f_{i,q} \tag{27}$$

where the $f_{i,q}$ are on the order of a few percent or less, and depend on the flight time of channel i. In the conventional mode the measured events are given by signal plus background,

$$O'_i = \ell'(S_i + F_i) = \ell'(S_i + \sum_{q<i} S_q\, f_{i,q}) \ . \tag{28}$$

In the PRBS mode the situation is slightly more complicated. Replacing S in Eq. (6) by S + F, with F as given in Eq. (27), gives

$$Z_k^n = \ell \sum_{j=0}^{N-1} S_{k+jN_b}\, a_{n-j} + \ell \sum_{j=0}^{N-1} \sum_{q<k+jN_b} S_q\, f_{k+jN_b,q}\, a_{n-j} \ . \tag{29}$$

Inversion of Eq. (29) via multiplication by $\{a^*_{n-j}\}$ gives the measured number of counts in TOF channel $i = k+jN_b$

$$O_i = \ell\left(S_i + \sum_{q<i} S_q\, f_{i,q}\right) . \tag{30}$$

Comparison of this equation with Eq. (28) for the conventional mode shows that PRBS pulsing gives no reduction of the "fitted" background as long as it remains correlated with the modulated flux.

C. Other Considerations

1. Unequal channel widths

Thus far we have assumed all channel widths to be of equal time duration. However, standard practice at ORELA is to bin the data into channels of varying duration which can be accomplished in the PRBS mode by summing over the appropriate time-spans.

Let $Z_k^{(n)}$ represent the events counted by the detector at time $(k+nN_b)\theta$. The observed number of events in TOF channel $k+jN_b$ of width θ is given by Eq. (7)

$$O_{k+jN_b} = \frac{2}{N+1} \sum_{n=0}^{N-1} Z_k^{(n)}\, a^*_{n-j} \ , \tag{31}$$

and the variance for this TOF channel is given by Eq. (9)

$$\mathrm{Var}(O_{k+jN_b}) = \left(\frac{2}{N+1}\right)^2 \sum_{n=0}^{N-1} Z_k^{(n)} \quad . \tag{32}$$

Let Q_α represent the observed number of events in bin α at time t_α°, of width τ_α. This bin is a combination of several of the original equal-width TOF channels numbers r_α to $r_{\alpha+1}-1$, so that the events in bin α are given by

$$Q_\alpha = \sum_{r=r_\alpha}^{r_{\alpha+1}-1} O_r \tag{33}$$

and the variance by

$$\mathrm{Var}(Q_\alpha) = \sum_{r=r_\alpha}^{r_{\alpha+1}-1} \mathrm{Var}(O_r) \quad . \tag{34}$$

In practice the conversion from channels to bins represents no significant complication. When the detector system observes an event contributing to $Z_k^{(n)}$ at time $(k+nN_b)\theta$, an event should be added to or subtracted from all TOF channels $k+jN_b$, according to Eq. (31). Rather than store all NN_b channel values O_{k+jN_b}, however, the computer simply adds or subtracts an event from the appropriate TOF bins α, according to Eq. (33). In addition, the computer may store the variances $\mathrm{Var}(Q_\alpha)$, since these quantities cannot be generated exactly from the bin counts alone. Storage requirements for the PRBS mode are therefore double the requirements for the conventional mode. Alternatively, only the TOF bin

counts Q_α may be stored, and postprocessing programs may be used to approximately regenerate O_{k+jN_b}, from which all other relevant quantities can be produced. In particular, it may be necessary to regenerate $Z_k^{(n)}$ in order to properly apply deadtime corrections.

2. Simultaneous experiments

Practical ORELA operation requires several simultaneous but different experiments which most likely will use the same PRBS. Therefore, the period N of the PRBS will not be optimum for all experiments; however, except for uncorrelated background, this is of little consequence.

For a single experiment the period N would be chosen to be as small as possible, in order to minimize computation, and still satisfy the inequality $NT_b \geq T_s$. When two experiments are run simultaneously, N is chosen to satisfy $N T_b \gtrsim T_s$ for the larger value of T_s; however, a smaller period, $\bar{N}$, would be adequate for the second experiment since for this measurement the S_{k+jN_b} are zero for $j > \bar{N}$. The counts measured by this detector include those zero-values channels:

$$Z_k^{(n)} = \ell d + \sum_{j=0}^{N-1} \ell S_{k+jN_b}\, a_{n-j} = \ell d + \sum_{j=0}^{\bar{N}-1} \ell S_{k+jN_b}\, a_{n-j} \tag{35}$$

where $\ell = T/T_b N$. Evaluation of TOF channel events need be done only for nonzero channels,

$$\ell d \frac{2}{N+1} + \ell S_{k+jN_b} = \frac{2}{N+1} \sum_{n=0}^{N-1} Z_k^{(n)}\, a^*_{n-j} \quad , \; 0 \leq j < \bar{N} \tag{36}$$

with the summation covering the entire range $0 \leq n < N$. The variance may be similarly evaluated as

$$\mathrm{Var}\left(\ell d\,\frac{2}{N+1} + \ell S_{k+jN_b}\right) = \left(\frac{2}{N+1}\right)^2 \sum_{n=0}^{N-1} Z_k^{(n)} \tag{37}$$

which is equivalent to

$$\mathrm{Var}\left(\ell d\,\frac{2}{N+1} + \ell S_{k+jN_b}\right) = \frac{4N}{(N+1)^2}\,\ell d + \frac{2}{N+1} \sum_{j^\circ=0}^{\bar{N}-1} \ell S_{k+j^\circ N_b} \,. \tag{38}$$

If this second experiment had been done using a PRBS period of $\bar{N}$ rather than N, the variance would be given by

$$\mathrm{Var}\left(\bar{\ell} d\,\frac{2}{\bar{N}+1} + \bar{\ell} S_{k+jN_b}\right) = \frac{4\bar{N}}{(\bar{N}+1)^2}\,\bar{\ell} d + \frac{2}{\bar{N}+1} \sum_{j^\circ=0}^{\bar{N}-1} \bar{\ell} S_{k+j^\circ N_b} \tag{39}$$

where $\bar{\ell} = T/T_b\bar{N}$. Comparison of Eqs. (38) and (39) shows that without uncorrelated background, results are approximately the same with the two values of the period; the ratio of the relative statistical errors is $\left[\frac{N}{N+1} \times \frac{\bar{N}+1}{\bar{N}}\right]^{1/2}$. For N = 255 and $\bar{N}$ = 31 this factor gives an increase of only 1.4% in the RSE for the larger period. However, the contribution of uncorrelated background to the signal is reduced by approximately $\bar{N}/N$ when the larger period is used.

3. Resolution time

Energy resolution is not affected by the introduction of the present PRBS pulsing scheme to ORELA. To see this, consider first the conventional mode. A schematic description of the neutrons reaching the detector during time period t_i to t_{i+1} is shown in Fig. 3. The source-to-detector flight time for an individual neutron is $t_i - \nu + \mu$, where ν is the source departure time as measured from the beginning of the channel. The total number of counts observed in this channel is

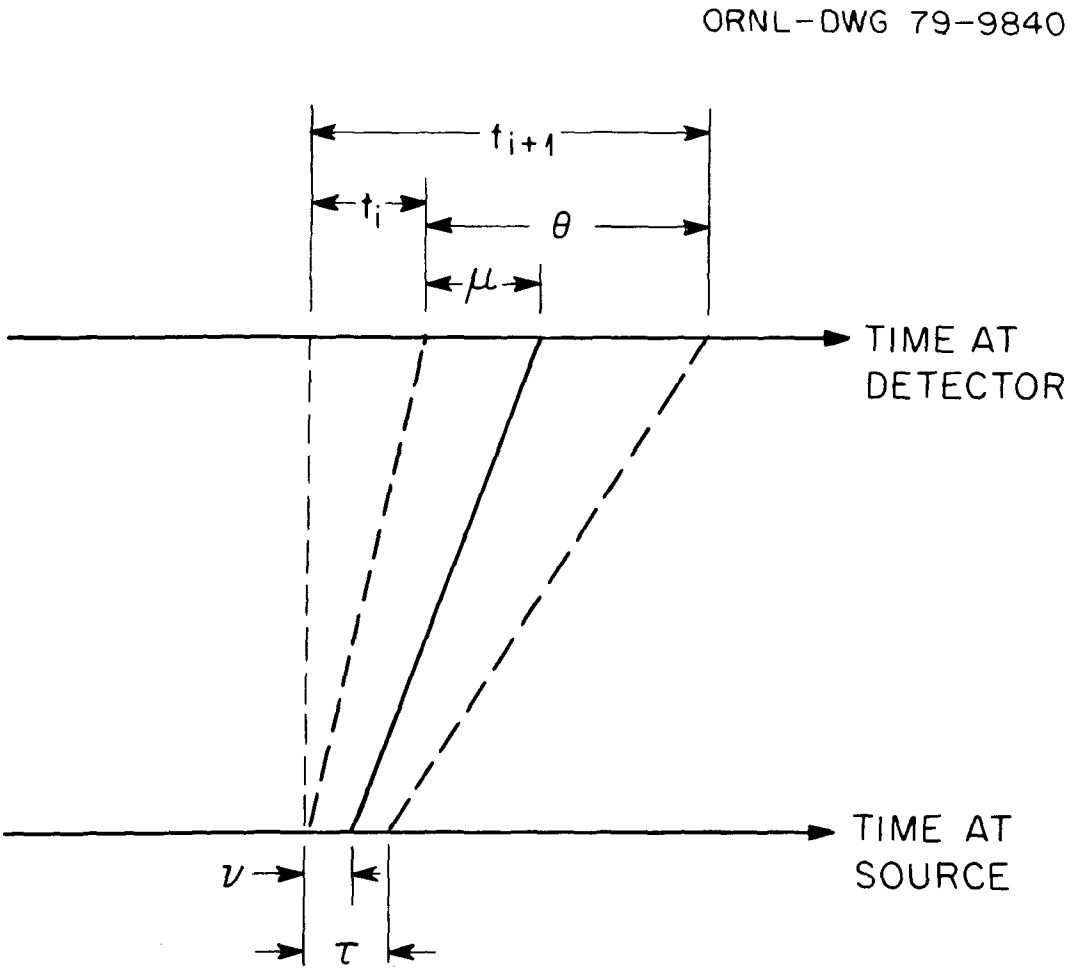

Fig. 3. Time sequence for resolution function. Source neutron pulses of width τ produce events in detector time channels of width θ.

$$S_i = \int_0^{\tau} d\nu \int_0^{\theta} d\mu \; s(t_i - \nu + \mu) \tag{40}$$

where s(t) is the number of neutrons per unit time with flight time t. Thus, the i^{th} channel records neutrons with flight times as low as $t_i - \tau$ and as high as $t_i + \theta$.

Consider now the PRBS mode. The description is similar, but contributions from many pulses reach the detector simultaneously. The analogous equation is

$$Z_k^{(n)} = \int_0^{\tau} d\nu \int_0^{\theta} d\mu \sum_{j=0}^{N-1} s(t_{k+jN_b} - \nu + \mu) \; a_{n-j} \tag{41}$$

where $t_{k+jN_b} = (k+jN_b)\theta$. Interchanging integrals with sums, Eq. (41) may be rewritten as

$$Z_k^{(n)} = \sum_{j=0}^{N-1} \left[\int_0^{\tau} d\nu \int_0^{\theta} d\mu \; s(t_{k+jN_b} - \nu + \mu) \right] a_{n-j} \; . \tag{42}$$

The quantity in square brackets is exactly S_{k+jN_b}. It follows that the time and hence energy resolutions in the PRBS and conventional modes are identical.

IV. COMPUTER MODELS OF TWO TIME-OF-FLIGHT EXPERIMENTS

In this section the expected TOF spectra for two typical measurements are calculated using the equations developed in the previous section assuming ORELA operation in both conventional and PRBS pulsing modes. In the first example a 20-meter ^{233}U fission cross section measurement is studied, employing realistic forms for the energy-dependent cross section and flux; however, the background is assumed zero. In the second example a ^{238}U 155-meter transmission measurement is studied with realistic backgrounds, but rather simple mathematical forms for the energy-dependent quantities. In the first example the experimenter is primarily interested in peaks and the smooth cross section at very low energies; in the second example the experimenter is primarily interested in transmission dips and the smooth cross section at very high energies.

A. 20-meter ^{233}U Fission Cross Section Measurement

The measurement of the ^{233}U fission cross section down to thermal energies is typical of many experiments performed at ORELA. Usually such measurements are done at 25 pulses per second (pps) on 20-m flight paths, so that a minimum energy of 0.00131 eV can be measured before frame overlap occurs. At 20 meters with no beam filters the flux and its correlated background have essentially vanished at this energy. Two models of this TOF spectra are generated and compared for data accumulation times of 24 hours; one model is for a 25 pps conventional measurement and the other for a 775 pps PRBS measurement with N = 31. Constant channel widths are used; backgrounds are assumed to be negligible; and deadtime, multiple scattering, and other complicating corrections are ignored.

In the conventional mode, the detector response can be written as

$$S(E) = n\varepsilon\sigma(E)\ \phi(E)$$

where n = nuclei/cm^3, ε = detection efficiency, $\sigma(E)$ = cross section, and $\phi(E)$ = fluence per second of channel width per burst per cm^2. The ENDF/B-IV ^{233}U fission cross section,[5] Doppler broadened to room temperature, was employed. This cross section is plotted on page 442 of Ref. 9. A 95% efficient fission chamber is employed with 0.243 gm of ^{233}U exposed to the flux. Assuming a 5.1-cm diameter beam spot, the correction for flux attenuation was $\lesssim$ 5% and was ignored. The flux $\phi(E)$ was obtained from log-log interpolation along a curve obtained from a 20-m, full power measurement which is documented in an internal correspondence dated April 22, 1970, from L. W. Weston to C. E. Bemis.[10] This flux was naively extrapolated from 0.0013 eV to 0.010 eV and from 100.0 keV to 10 MeV following the same energy dependences documented from 0.01 eV to 0.03 eV and 1.0 eV to 100.0 keV, respectively. It is important to appreciate the rapid increase in flux with increasing neutron energy for fixed-time channel widths. For example, the flux per second of channel width is 6000 times larger at 100.0 keV than at 1.0 eV. Multiplication gives a count rate of $S_i = 5.9 \times 10^4\ \phi(E)\ \sigma(E)$ per second of channel width per burst.

The lower parts of Figs. 4 to 7 show this count rate normalized for a 24-hour conventional measurement calculated over 266667 150-nsec wide channels for times from 450 nsec to 40 msec, which correspond to incident neutron energies from 10 MeV to 0.0013 eV. Since there is no background, the RSE for this measurement is simply the inverse square root of the ordinate. The results shown in Fig. 4 (0.8 msec to 40 msec) have been averaged by a factor of 205 for plotting purposes.

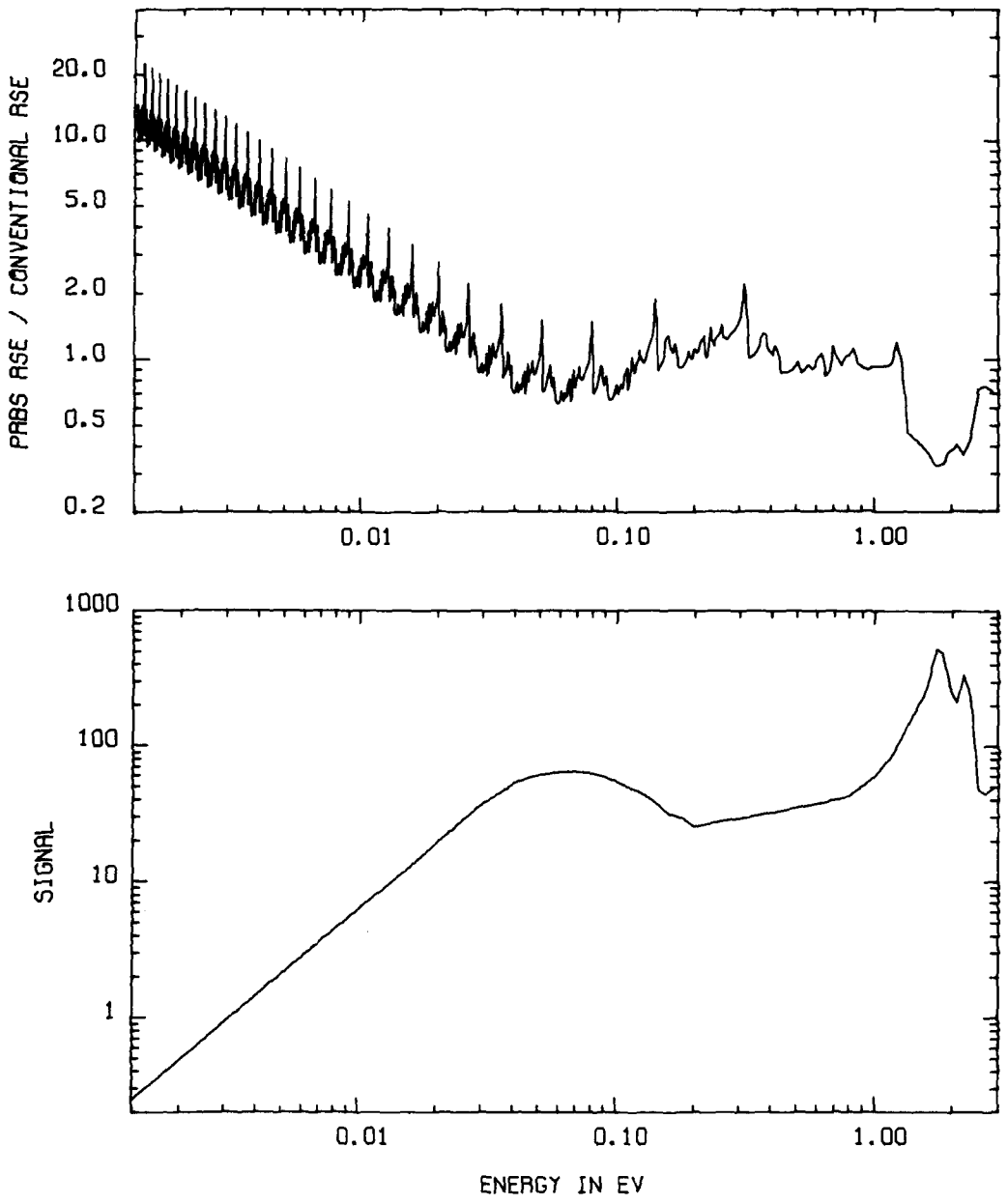

Fig. 4. Computer-calculated ^{233}U fission chamber spectrum for 0.00137 to 3.0-eV neutrons. The upper curve is the RSE from the PRBS pulsing divided by the RSE from the conventional pulsing. The sharp peaks on this ratio are from MeV neutrons.

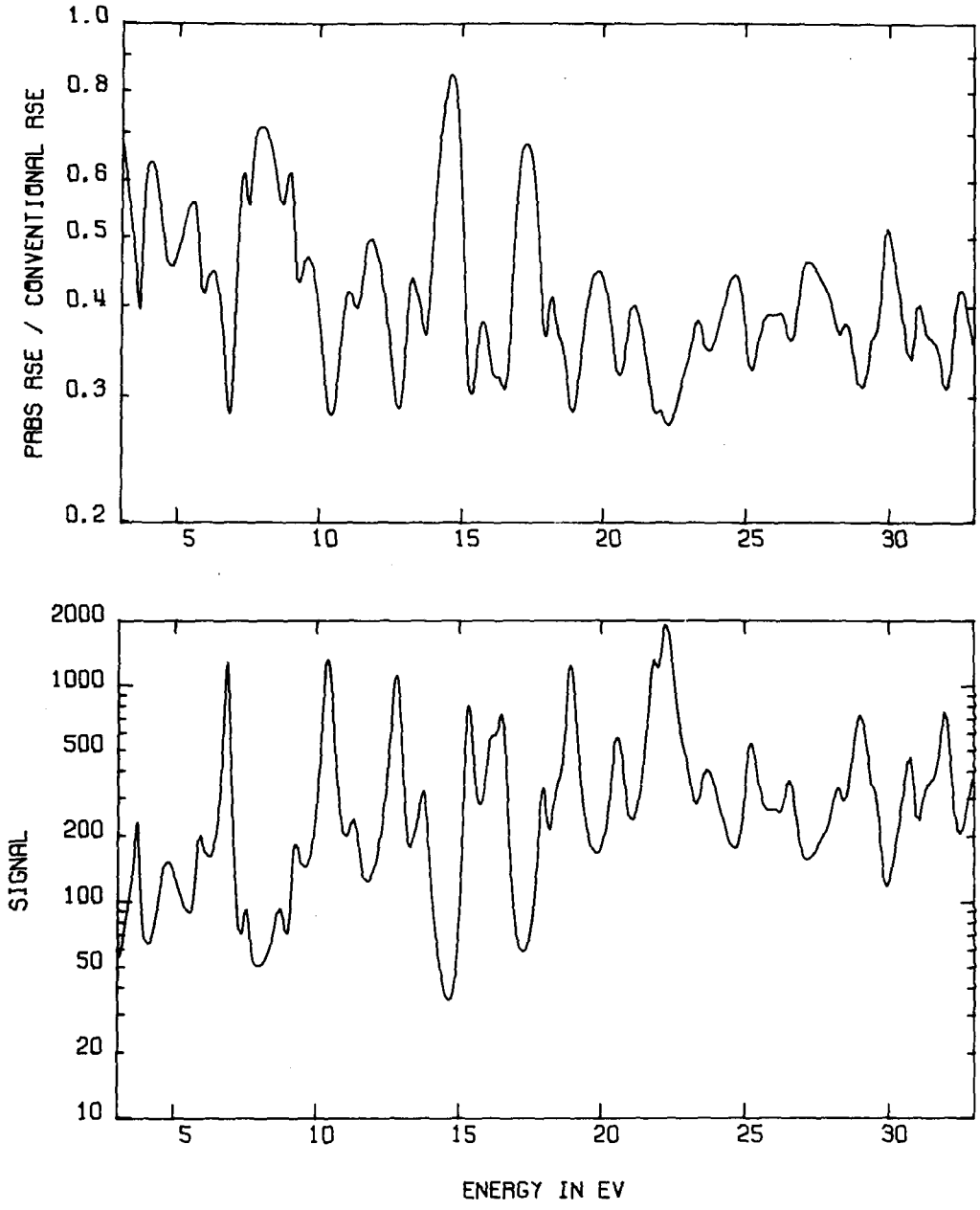

Fig. 5. Computer-calculated ^{233}U fission chamber spectrum for 3.0 to 33.0-eV neutrons. The upper curve is the RSE from the PRBS pulsing divided by the RSE from the conventional pulsing.

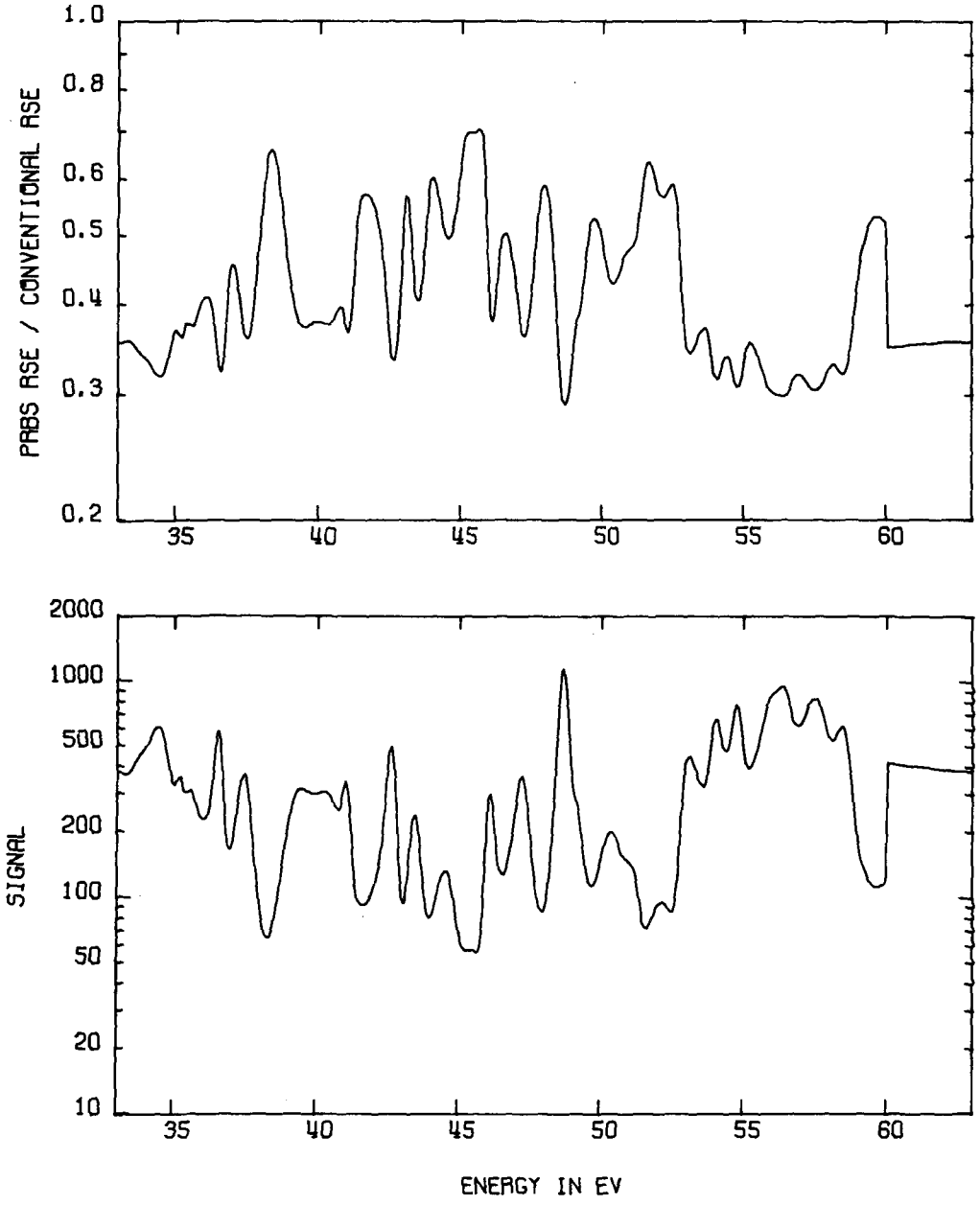

Fig. 6. Computer-calculated ^{233}U fission chamber spectrum for 33.0 to 63.0-eV neutrons. The upper curve is the RSE from the PRBS pulsing divided by the RSE from the conventional pulsing.

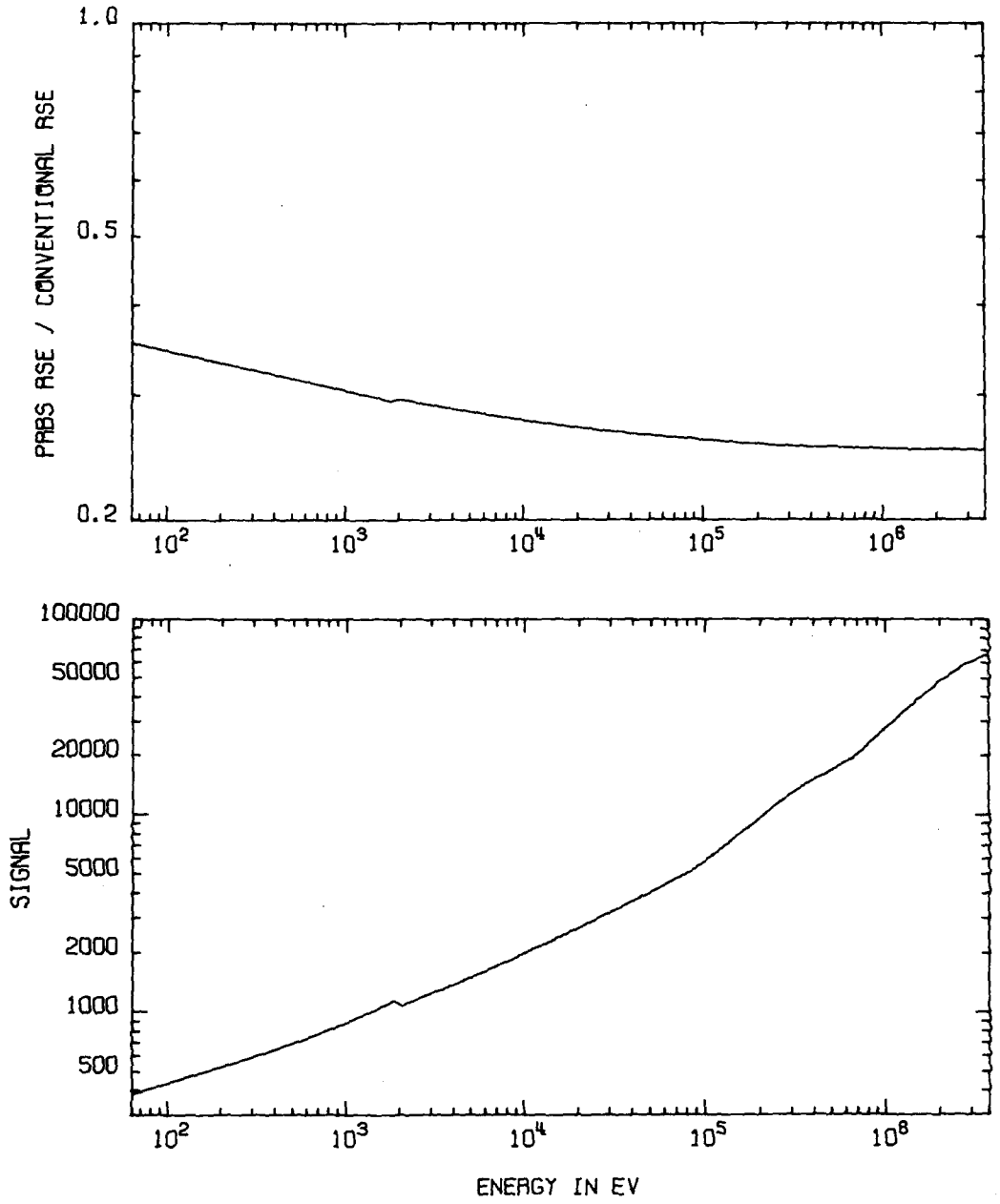

Fig. 7. Computer-calculated ^{233}U fission chamber spectrum for 63.0-eV to 3.7-MeV neutrons. The upper curve is the RSE from the PRBS pulsing divided by the RSE from the conventional pulsing. At very high neutron energies this ratio approaches its minimum value, maximum gain for PRBS, of $\sqrt{2/(N+1)} = 0.25$.

In actual operation in the PRBS mode, ORELA would be pulsed at the maximum repetition rate of $\sim$ 1000 pps; in order to accommodate the maximum flight path length of 200 m, a PRBS of period N = 511 would be required. Even with the channel width as large as 150 nsec, this would require 4.4×10^6 storage locations if the intermediate spectrum $Z_k^{(n)}$ were to be saved. In practice what would be stored is probably not $Z_k^{(n)}$, but rather the unfolded signals for the unequal-width TOF bins as described in the previous section. However, in order to generate and display $Z_k^{(n)}$ explicitly for this example, a repetition rate of 775 pps and a PRBS of period N = 31 were used. As indicated in the previous section, no substantial differences result from this; all advantages and disadvantages of PRBS pulsing with respect to conventional pulsing are essentially identical for the two values of N.

Using the same definition of signal S as was used in the conventional mode, the detector response $Z_k^{(n)}$ was generated according to Eq. (6) with N = 31 and N_b = 8610. This intermediate spectra is shown in Fig. 8 in which results have been averaged over approximately 100 channels for plotting purposes. Because no uncorrelated backgrounds are present, the unfolded PRBS spectrum is identical to the conventional spectrum to within a normalization and is not plotted separately.

Because this example did not include any background components, the only valid criterion for comparing results from the two pulsing modes is the ratio of their relative statistical uncertainties. Such a comparison is shown in the upper curves of Figs. 4 to 7, which picture the ratio R, Eq. (15), of the RSE for the PRBS measurement to the RSE from the conventional measurement. If R is greater than unity, the conventional

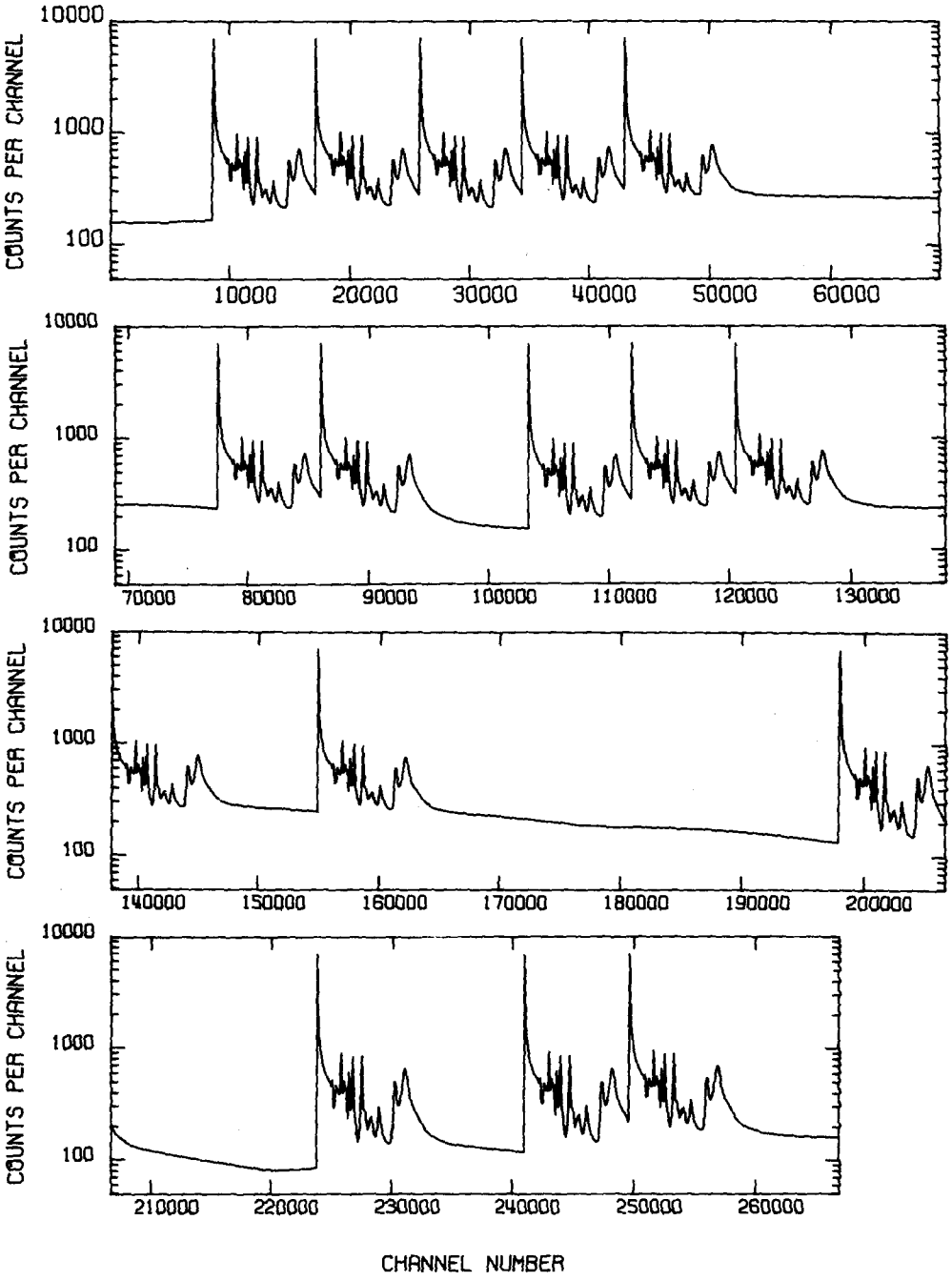

Fig. 8. Calculated detector response through one N = 31 PRBS for the ^{233}U fission chamber measurement. The calculated results have been compressed by a factor of 100 for plotting.

mode is superior; and if R is less than unity, the PRBS mode is superior. Figure 7 shows this ratio monotonically decreasing from 0.34 at 63 eV to 0.25 at 3.7 MeV; the value 0.25 is the maximum gain available from PRBS pulsing with repetition rate 31 times that of the conventional mode. In particular, the calculated signal at 3.7 MeV is 75,000 which overlaps with a signal of $\sim$ 100 at 1.26 eV, a signal of $\sim$ 30 at 0.31 eV, etc. Consequently, the requirements for Eq. (16) are met and $R = \sqrt{2/(N+1)} = 0.25$.

The ratio of RSE over the resolved resonance region from 3 to 63 eV is shown in the upper curves of Figs. 5 and 6. This ratio varies between $\sim$ 0.3 and $\sim$ 0.9, indicating that the PRBS pulsing is superior at all those energies. At the resonance energies the ratio approaches 0.25, the theoretical limit, and in the valleys between resonances the ratio approaches but never exceeds unity. Peaks in the signal correspond to valleys in the ratio and vice versa.

Figure 4 shows the ratio of RSE from 0.00137 to 3.0 eV, the energy range of interest for thermal reactors. The overlapping pulses of the PRBS measurement are apparent in the ratio, where the largest periodic peak corresponds to overlap with MeV-neutron produced fissions. It is important to realize that a gamma-flash overload problem could destroy the signal at every energy where this peak occurs. The two peaks directly above this high-energy overlap signal are from the 1.8 and 2.3 eV doublet. Structure intermediate between these disappear in the averaging process required for plotting. For energies above $\sim$ 0.04 eV, on the average the PRBS mode is more or less equivalent to the conventional mode except for the 1.8 - 2.3 MeV doublet. Below $\sim$ 0.04 eV the conventional mode is clearly superior.

If a significant uncorrelated background had been included in this model, PRBS pulsing would effectively reduce that background by a factor of (N+1)/2 or 16 with N = 31. This in turn would reduce the ratio R. In addition, we have assumed that the minimum time between pulses limits ORELA; however, if the average power were the only limit for ORELA, the PRBS-mode repetition rate could be increased by a factor of 2, and the ratio R would be further reduced by a factor of $\sqrt{2}$.

B. 155-meter ^{238}U Transmission Measurement

For this example the sample-in spectra for a simplified 155-m ^{238}U transmission measurement are simulated and compared for two conventional modes and one PRBS mode of ORELA pulsing. The first mode employs a 1.53 gm/cm^2 ^{10}B time overlap filter and a pulse repetition rate of 200 pps, both of which were used to make the measurement described in Ref. 6; with respect to time overlap this is a difficult measurement. The second conventional mode employs no time overlap filter; this gives a thermal normalization, but requires a pulse rate of 3.22 pps. The third mode uses PRBS pulsing at 800 pps with N = 511 and no time overlap filter.

For a sample-in transmission measurement the signal per burst per second of channel width, without background, can be written as

$$S(E) = \phi(E)\ T_B(E)\ \varepsilon(E)\ T_S(E)\ , \tag{43}$$

where $\phi(E)$ = fluence per burst per second of channel width, $T_B(E)$ = transmission of the ^{10}B filter if used, $\varepsilon(E)$ = detector efficiency, and $T_S(E)$ = sample transmission. In order to reduce the complexity and length of the calculation, simplified forms were used to approximate these energy-dependent quantities. The resulting spectra were not resolution broadened.

Again the flux curve of Ref. 10 was employed, multiplied by the factor 0.062 to give the expected fluence per burst per second of channel width at half power for a 7.9-cm diameter beam spot at 155 m after attenuation by a 7.2 gm/cm^2 Pb filter. This factor contains a 50% increase to reproduce the measured fluence at 3524 eV.[6] For the first conventional mode the attenuation through a 1.53 gm/cm^2 (0.0918 atom/barn) ^{10}B filter was required; the ^{10}B total cross section, taken from Ref. 11, gives a transmission of

$$T_B(E) = \exp[-0.0918(2.43+611.0\ E^{-1/2})] \ . \tag{44}$$

For the other two modes $T_B(E) \equiv 1.0$. It was assumed that neutrons were detected with a $\sim$ 13-mm thick Li-glass disk whose detection efficiency was proportional to $1/\sqrt{E}$ and had a value of 15% at 1.0 keV. Ignoring all other complications, this gives

$$\begin{aligned} \varepsilon(E) &= 4.47\ E^{-1/2} \quad \text{for } E \geq 22.47 \text{ eV} \\ &\quad 1.0 \qquad\quad \text{for } E \leq 22.47 \text{ eV} \ . \end{aligned} \tag{45}$$

Neutron attenuation through the sample was determined with the usual equation

$$T_S(E) = \exp[-n\sigma(E)] \tag{46}$$

where n is the sample areal number density which was taken as 0.0124 atoms/barn (22.5 mm of ^{238}U). The Doppler broadened total cross section was simplified to reduce the complexity of calculating 511 overlapping signals with a varying TOF bin structure; $\sigma(E)$ was assumed to have 11.2

barns of potential scattering with symmetric Breit-Wigner resonances including Doppler broadening at decimal intervals from 0.1 eV to 0.1 MeV; that is,

$$\sigma(E) = 11.2 + \sum_{i=1}^{7} \frac{A_i}{(E-E_i)^2+B_i} . \qquad (47)$$

Because the Doppler FWHM, 0.035 $\sqrt{E}$ eV, is much larger than the average neutron width, 0.0029 $\sqrt{E}$ eV, the resonance FWHM, $2\sqrt{B_i}$, was taken to be the quadratic sum of the Doppler width and a 0.023 eV radiation width. Neutron widths were adjusted to give a maximum cross section A_i/B_i of 230.4 barns, resulting in a minimum transmission of 0.05. Parameters E_i, A_i, and B_i are given in Table 1, along with the transmission of the ^{10}B at the resonance energies and the assumed TOF bin width over the transmission dip. Three backgrounds were employed whose time dependences and magnitudes with respect to the measured signal approximate those subtracted from the ^{238}U transmission spectra of Ref. 6. First, the detector registered 8 cts/sec of room background, independent of the ORELA flux. Second, the Li glass detected a background of 658 exp (-.0385 t) cts/sec/burst where t is clock time in seconds. This background results from gamma rays from H capture in the ORELA target-moderator and is correlated with the ORELA flux. Third, the detector response to room return was taken to be 2% of the average flux measured by the Li glass, or 1.7% of the flux preceding the transmission sample; this beam-correlated background approximates the fitted background of Eq. (27).

TABLE 1. Cross Section Parameters For Transmission Calculation

E_i (eV)	A_i	B_i	T_B (E_i)	Δt	FWHM (eV)
0.1	0.03752	1.629×10^{-4}	0.000	4 msec	0.025524
1.0	0.1010	4.385×10^{-4}	0.000	65 μsec	0.041881
10.0	0.7361	3.195×10^{-3}	0.000	4096 nsec	0.11304
100.0	7.087	3.076×10^{-2}	0.003	256 nsec	0.35075
1.0×10^3	70.59	0.3064	0.136	32 nsec	1.1070
1.0×10^4	705.7	3.063	0.457	4 nsec	3.5001
1.0×10^5	7055.	30.62	0.670	0.5 nsec	11.068

Figures 9 to 15 display the calculated results. The lower part of each figure shows the calculated spectra over the decimal-interval transmission dips. These are not final transmissions but sample-in spectra, all normalized to $\sim$ 0.87 near the right-hand edge of the figure. The histogram is the 3.22 pps no-boron spectrum; the smooth curves are the 200 pps spectrum with boron and the PRBS spectrum, where the curve with the lowest transmission dip is always the PRBS result. The upper figures are ratios of absolute statistical standard deviations, including background contributions, with the corresponding spectral normalizations. Thus, they reflect the ratios of the absolute statistical accuracy to which the lower spectra can be measured. The ratio labeled thermal is the PRBS spectral error divided by that of the 3.22 pps spectrum; the ratio labeled boron is the PRBS error divided by that of the 200 pps spectrum. Ignoring the merits of a decreased background and the statistical implications of its subtraction, a ratio greater than unity indicates the conventional mode is superior and a ratio less than unity indicates the PRBS mode is superior.

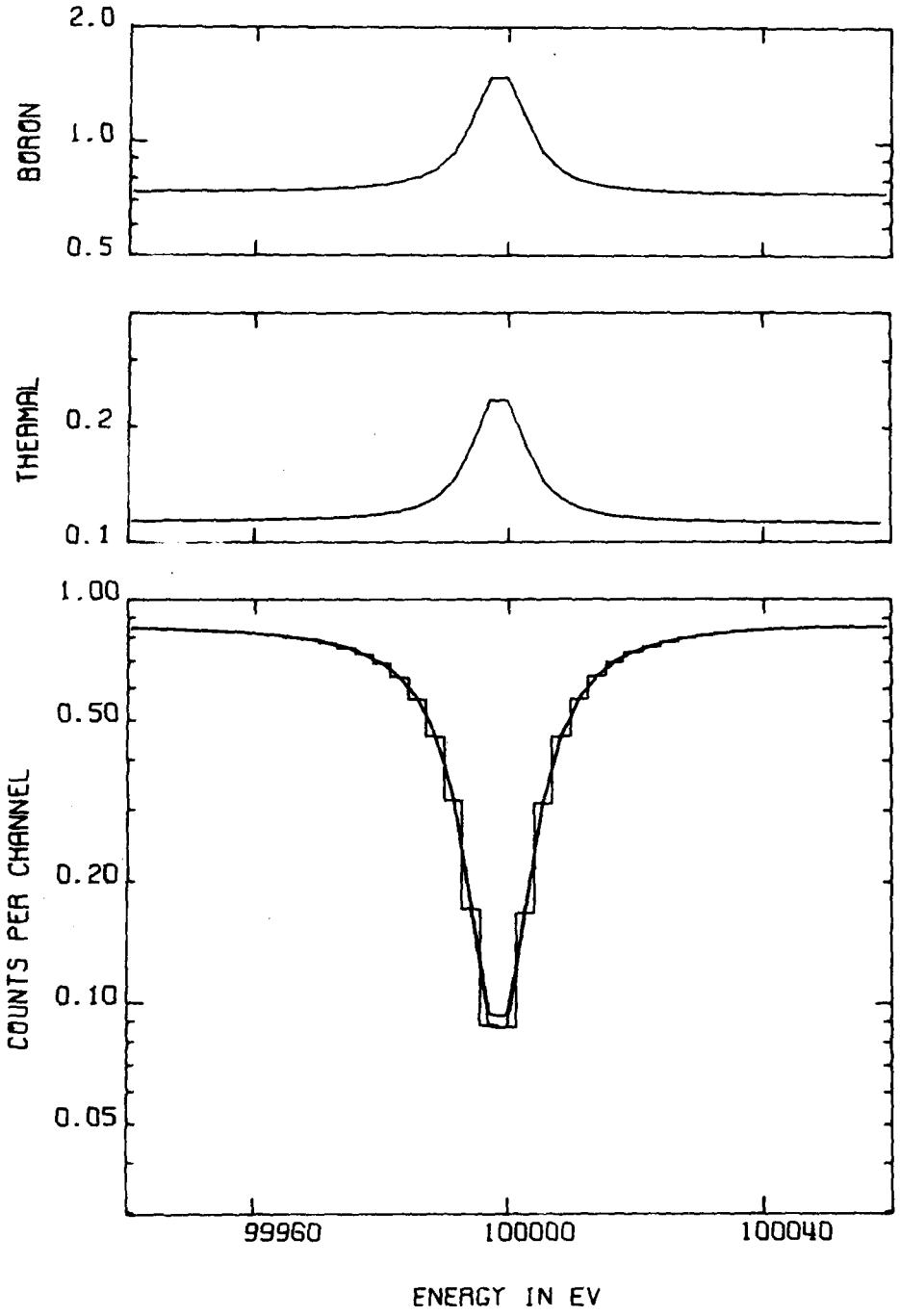

Fig. 9. Calculated ^{238}U transmission spectrum over the 100 keV resonance. The curve labeled "THERMAL" is the calculated statistical error of the PRBS mode divided by that for the 3.22 pps mode, whereas the curve labeled "BORON" is the corresponding ratio to the 200 pps mode.

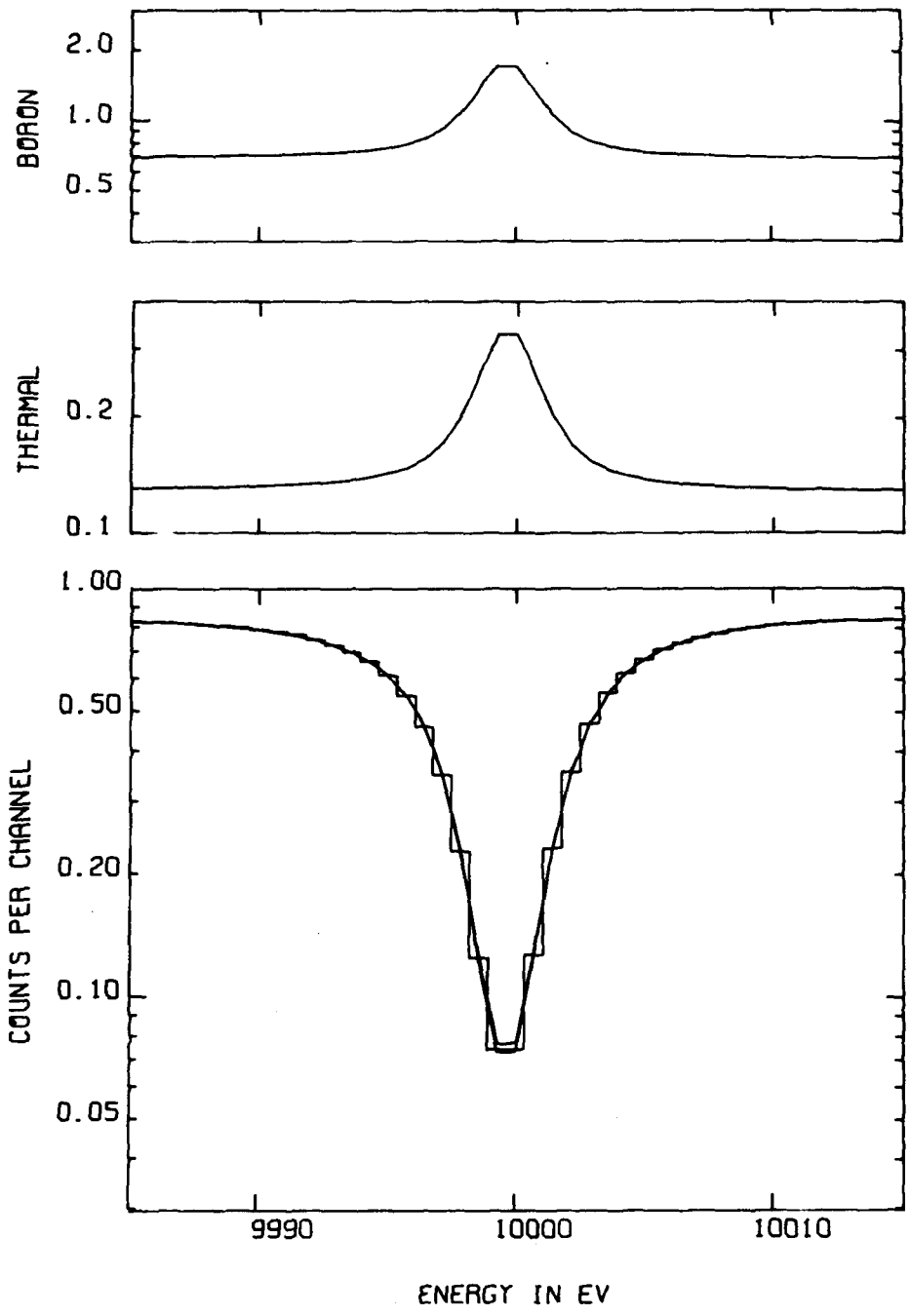

Fig. 10. Calculated ^{238}U transmission spectrum over the 10 keV resonance. The curve labeled "THERMAL" is the calculated statistical error of the PRBS mode divided by that for the 3.22 pps mode, whereas the curve labeled "BORON" is the corresponding ratio to the 200 pps mode.

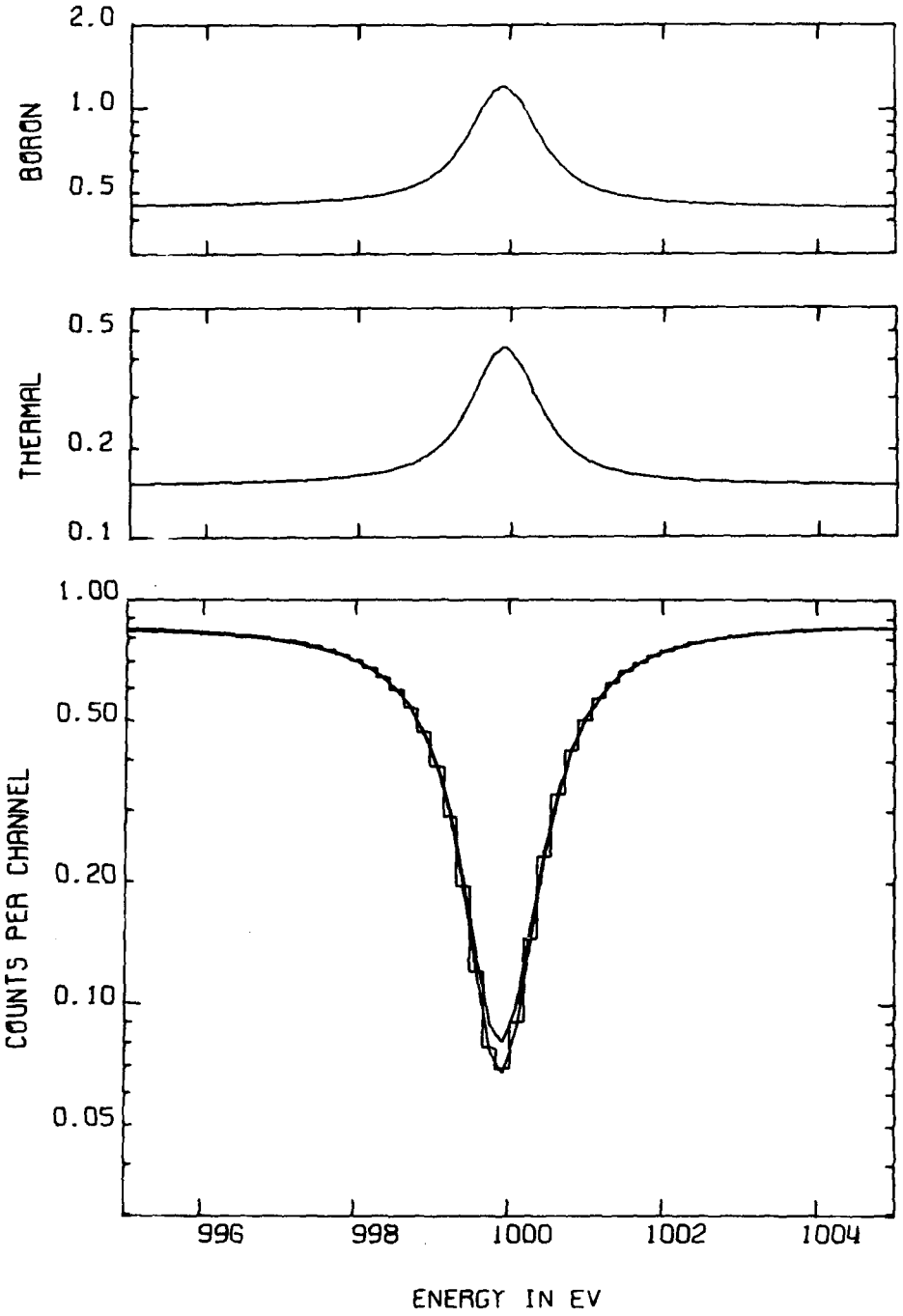

Fig. 11. Calculated ^{238}U transmission spectrum over the 1.0 keV resonance. The curve labeled "THERMAL" is the calculated statistical error of the PRBS mode divided by that for the 3.22 pps mode, whereas the curve labeled "BORON" is the corresponding ratio to the 200 pps mode.

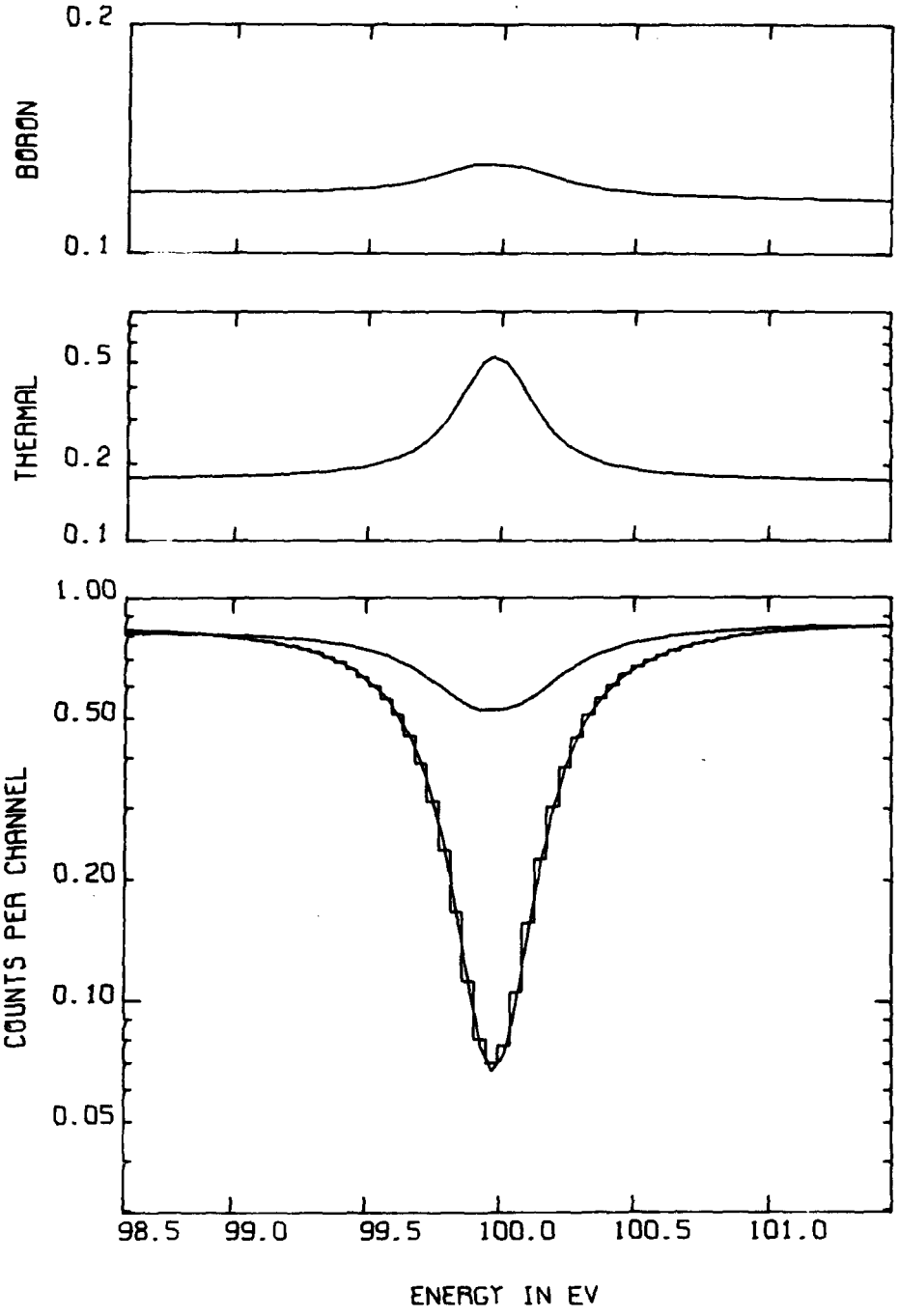

Fig. 12. Calculated ^{238}U transmission spectrum over the 100 eV resonance. The curve labeled "THERMAL" is the calculated statistical error of the PRBS mode divided by that for the 3.22 pps mode, whereas the curve labeled "BORON" is the corresponding ratio to the 200 pps mode.

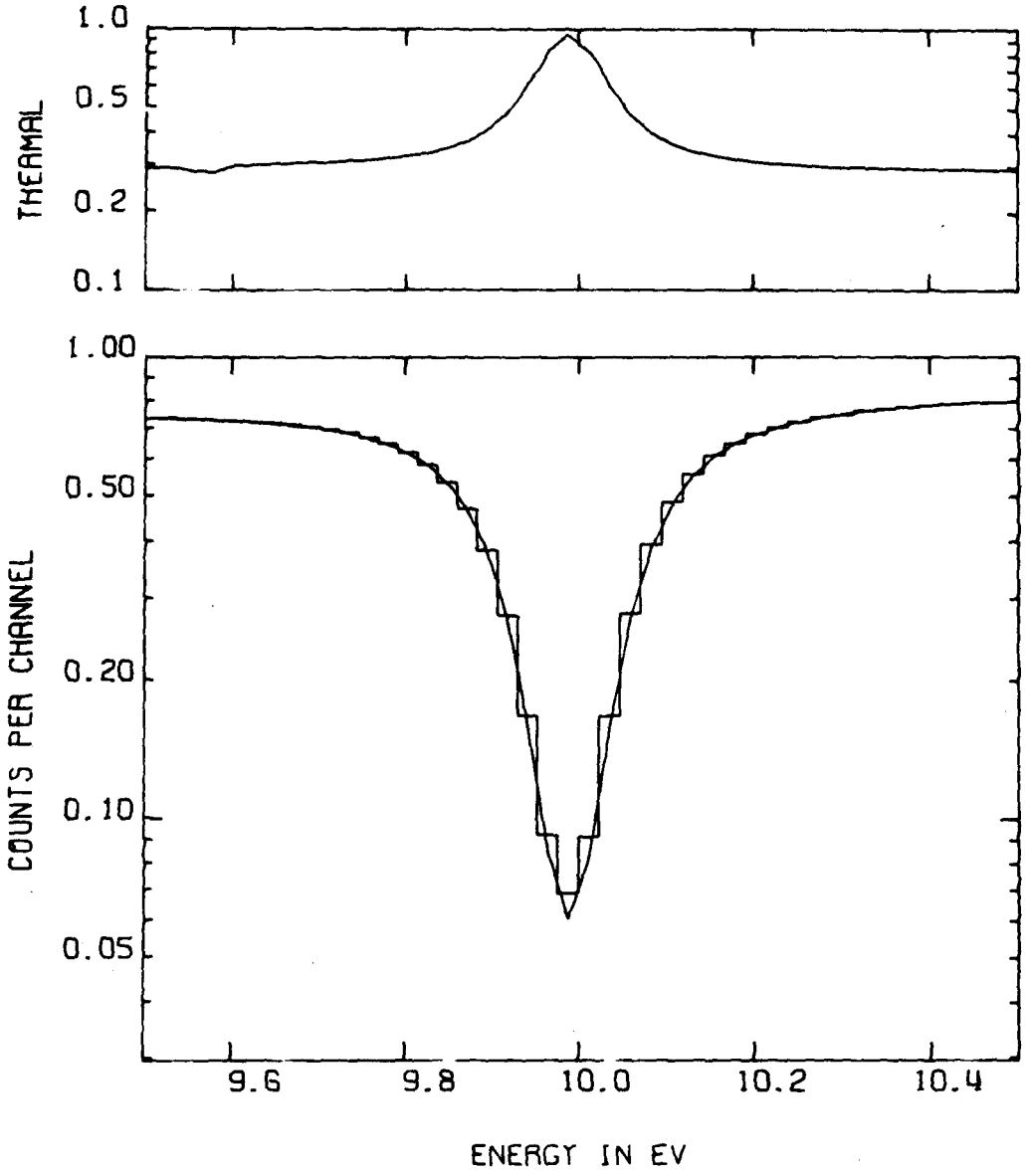

Fig. 13. Calculated ^{238}U transmission spectrum over the 10 eV resonance. The curve labeled "THERMAL" is the calculated statistical error for the PRBS mode divided by that for the 3.22 pps mode.

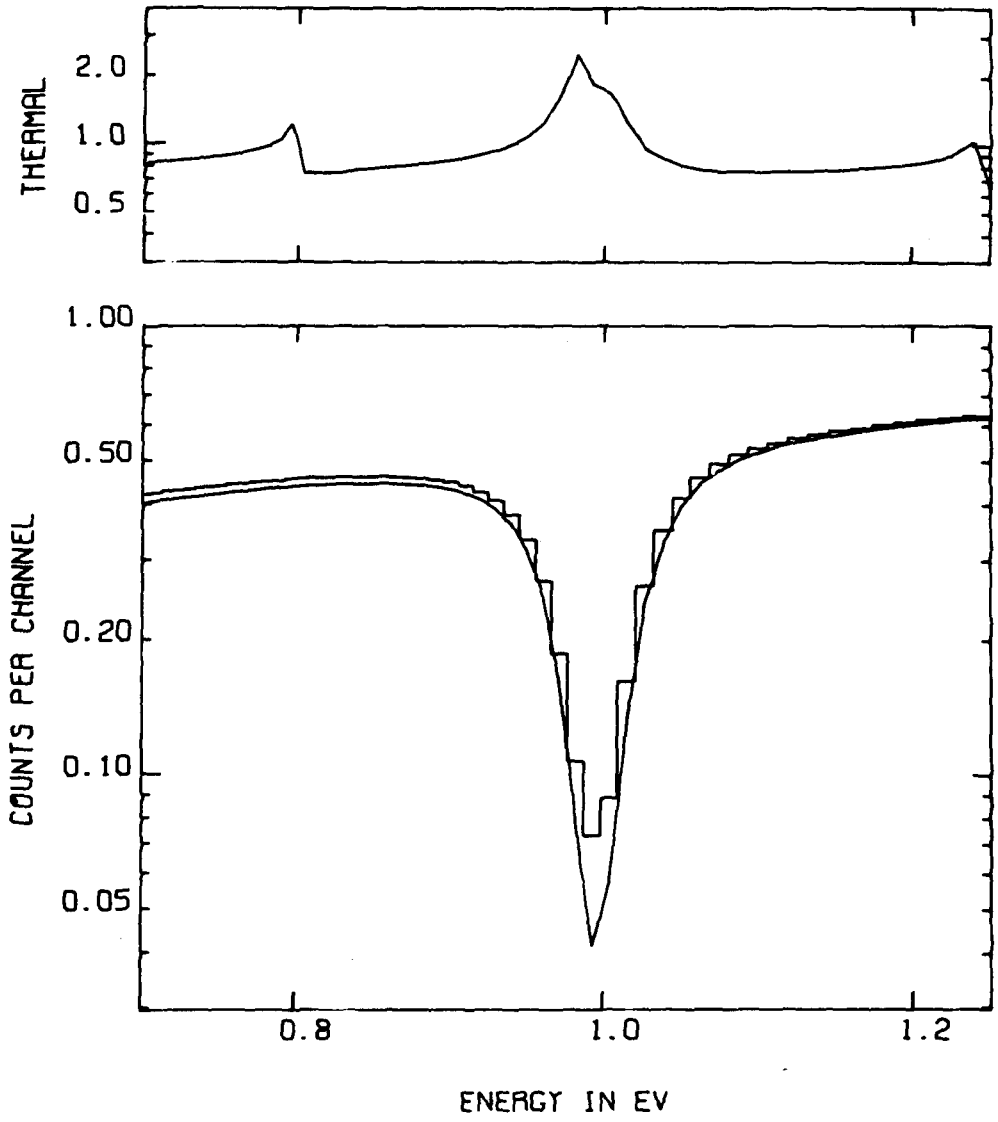

Fig. 14. Calculated ^{238}U transmission spectrum over the 1.0 eV resonance. The curve labeled "THERMAL" is the calculated statistical error for the PRBS mode divided by that for the 3.22 pps mode.

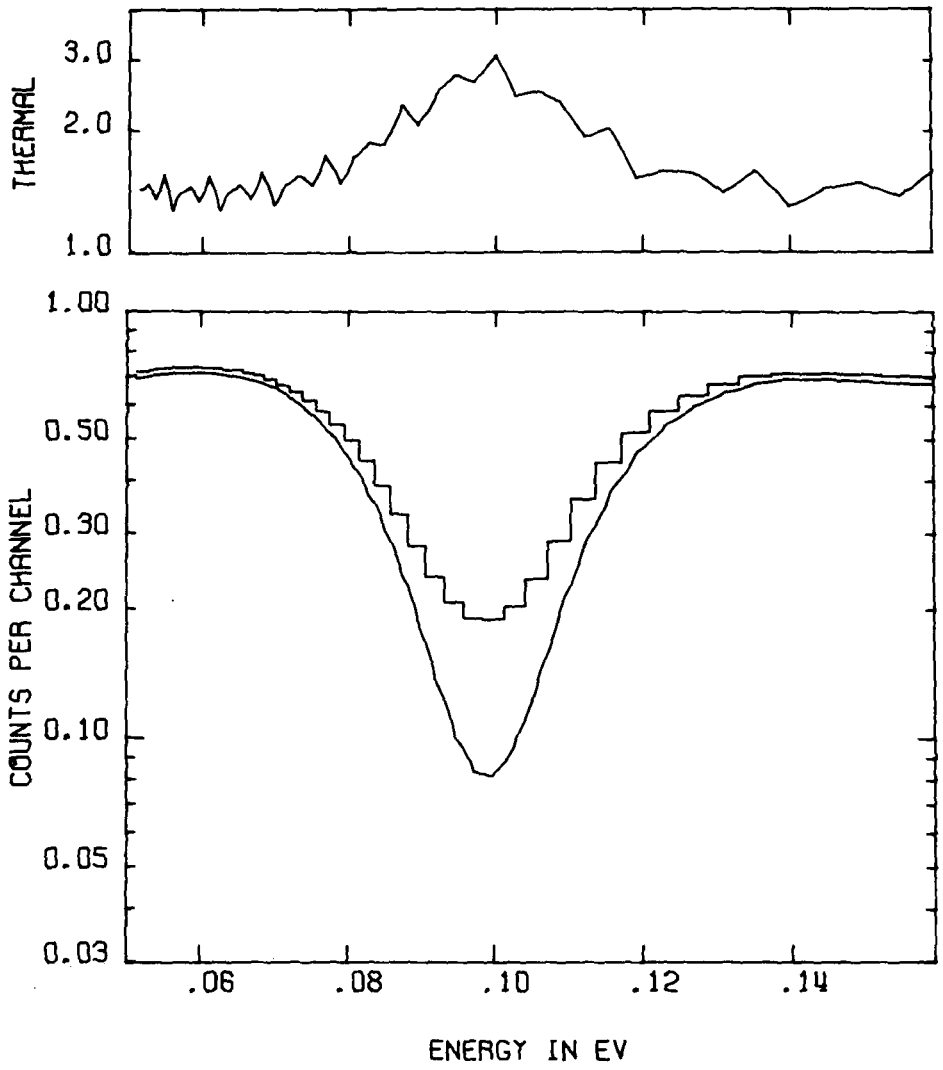

Fig. 15. Calculated ^{238}U transmission spectrum over the 0.1 eV resonance. The curve labeled "THERMAL" is the calculated statistical error for the PRBS mode divided by that for the 3.22 pps mode.

Figure 9 shows the spectra and the error ratios for the 100 keV resonance. Because the uncorrelated background is negligible, the three transmission dips are nearly identical. Even with boron-produced flux reduction of 0.67, the transmission minimum is most precisely determined via the 200 pps measurement, whereas the potential scattering cross section is more accurately obtained via the PRBS mode. At this energy the 3.22 pps thermal measurement has the largest absolute standard deviation by a factor of $\sim 0.16 = [3.22 \text{ pps}/(0.67 \times 200 \text{ pps})]^{1/2}$ when compared to the boron mode. Figures 10 and 11 show similar results for the 10 keV and 1 keV resonances, with boron attenuations of 0.46 and 0.14, respectively.

The resonances in this example were chosen to give calculated transmission dips of 0.05; additional counts in the minima are due to background. The time-independent background for the 3.22 pps and PRBS spectra in Fig. 11 is negligible; however, for the 200 pps measurement with boron attenuation of 0.14, the time-independent background contributes about 1% of the transmission minimum. If the resonances of Fig. 9 to 11 produced transmission minima less deep, the PRBS mode would appear more favorable; and if they produced deeper minima, the conventional mode would appear more favorable.

One major difficulty of transmission measurements is background determination, which can be verified only by resonances which give zero transmission minima. The 200 pps measurement was designed for neutron energies above 1 keV and on this crucial point is superior to the PRBS result. Although PRBS pulsing does reduce the 1 keV resonance background by $\sim$ 1%, this background is easily measured and accurately subtracted.

To gain further insight to the relative merits of PRBS pulsing, PRBS spectra are compared with the 3.22 pps measurement down to thermal energy in Figs. 12 to 15. Figures 12 and 13 show transmission dips for the 100 eV and 10 eV resonances; the 200 pps result is of no interest at these energies since the boron has attenuated the flux to nearly zero. The PRBS mode gives a smaller statistical error in both the transmission minima and the maxima than does the 3.22 pps mode but does not significantly reduce the background level. The slight minimum in the error ratio near 9.6 eV is caused by overlap with the 10 keV resonance.

If absolute error were the only basis for comparison, Figs. 14 and 15 show that the 3.22 pps conventional mode is superior to the PRBS mode. However, removal of the $\sim$ 14% uncorrelated background under the 0.1 eV resonance is an obvious and important advantage of the PRBS mode. The maxima in the error ratio at 0.80, 0.99, and 1.25 eV in Fig. 14 are from overlap with the high-energy flux and correspond to positions of possible gamma-flash overload. Unfortunately one of these overlaps occurs in the transmission dip. In Fig. 15 these possible overloads occur every $\sim$ 0.01 eV, but a much smaller channel structure could isolate these potential problems.

V. SUMMARY AND CONCLUSIONS

The simplest application of pseudorandom binary sequence pulsing of ORELA involves superimposing a PRBS on the conventional equally spaced ORELA pulses at the maximum repetition rate. Approximately half the bursts and hence half the maximum ORELA flux may be discarded, but the resulting PRBS pulse pattern has characteristics which may compensate for this loss of flux. Neutrons from different bursts may time overlap at the detector and flux uncorrelated backgrounds would be greatly reduced.

Equations have been developed to describe this application of PRBS to ORELA. These equations describe the unfolding of the desired TOF spectra from the measured detector spectra, both without and with background. Variances and, in Appendix A, covariances for the TOF spectra are also described. This allows a quantitative comparison between expected results from PRBS and conventionally pulsed measurements. With no background, the ratio of relative statistical errors forms the basis for comparison. In general, c = 1/2 PRBS pulsing improves the RSE for TOF channels whose count rate is more than twice the average count rate of those TOF channels with which it overlaps. However, this gain is achieved at the expense of the RSE of the corresponding overlapping TOF channels with low count rates. In fact, without gains from filter removal and uncorrelated backgrounds PRBS pulsing cannot reduce the "average" variance with respect to conventional pulsing.

Foreground-correlated backgrounds were shown to be unaffected by PRBS modification of ORELA and therefore require no special treatment. However, detector overload as caused by the gamma flash would present a

problem. In the PRBS mode, information would be lost for all TOF durations overlapping the gamma flash. This should, however, be only a small fraction of the flight-time at low energies and may not constitute a significant problem.

It is with time-independent beam-uncorrelated background that the PRBS mode is most strikingly advantageous. Such backgrounds are reduced by a factor 2/(N+1). In TOF measurements with a reactor neutron source this background is often as large as the foreground; however, for ORELA experiments, this background is usually only a few percent of the foreground. Moreover, it is relatively easy to measure. Consequently, the reduction of uncorrelated backgrounds by PRBS pulsing is not sufficiently advantageous to warrant PRBS implementation. Nevertheless, for a few measurements this may be a significant advantage.

Computer models have been generated for two typical ORELA TOF measurements simulating spectra, background, and statistical errors for both PRBS and conventional modes. Comparison of the PRBS and conventional modes indicates that, in the absence of backgrounds, PRBS pulsing cannot enhance ORELA performance for measurements involving only high-energy neutrons, because 100% of the ORELA flux is employed directly in the conventional measurement. Surprisingly, PRBS pulsing also does not enhance ORELA performance for thermal measurements involving neutrons below $\sim$ 1 eV, at least for relatively flat cross section, since low energy signals per unit of time channel width are in general much smaller than the overlapping high energy signals.

In the intermediate resolved-resonance region, the many options for the conventional mode tend to confuse comparisons. Flight-path

length, time-overlap filters, and repetition rate can all be varied, and the trade-offs are not clear cut. Cadmium filters have a sharp cutoff at $\sim$ 0.5 eV but introduce resonance structure into the flux. Boron filters have a smooth transmission but usually filter out a significant fraction of the neutrons of interest. For the 20-m ^{233}U fission measurement at energies above $\sim$ 1.2 eV, the first overlap, PRBS pulsing is clearly superior to 25 pps conventional pulsing; however, this would not be the case compared to a 300 pps conventional Cd filter measurement. For the ^{238}U transmission measurement conventional pulsing seems to give less statistical uncertainty in the minima of black resonance transmission dips.

The primary advantage which PRBS pulsing introduces to ORELA experiments is simultaneity. An entire spectrum can be measured simultaneously, from thermal energies to the MeV region with maximum ORELA repetition rate. Results at all energies would be directly normalized to thermal cross section values without introduction of additional uncertainties from combining separate measurements. Since ORELA would always operate at maximum repetition rate, two distinct measurements which conventionally require different repetition rates could be run concurrently with PRBS pulsing. An experiment using maximum PRBS pulsing at the repetition rate in the conventional manner would suffer a $\sqrt{2}$ loss in RSE in the PRBS mode, but might gain additional run time to compensate this loss.

Results and conclusions described in this report have been based on specific assumptions regarding the nature of PRBS pulsing at ORELA. ORELA neutron bursts are assumed to be of equal intensity and equal time width. A maximum of 800 to 1000 uniformly spaced pulses per second can

be produced, on which is superimposed a PRBS whose period is sufficiently large to permit unfolding of time overlapping channels for all measurements which might be run concurrently. It is further assumed that this maximum repetition rate cannot be increased because of the PRBS pulsing; that is, the limiting factor is time between individual bursts rather than time-averaged power output.

From this study it is not obvious whether work on PRBS pulsing of ORELA should continue. To continue work on PRBS pulsing would require the following studies: First, detailed computer simulations of more typical ORELA experiments must be performed, primarily for those experiments which appear to have the most to gain or lose by switching to the PRBS mode. These simulations should include all complications described below and should use realistic signals and backgrounds. These PRBS simulations must be compared with simulations of the optimum conventional methods. Second, the implications of such details as variation in burst width and/or intensity, both correlated and uncorrelated to the PRBS sequence, must be theoretically understood. The exact versus approximate treatment of deadtime corrections must be examined both theoretically and with the aid of computer simulations. Appropriate algorithms should be established for generating and storing variances and covariances, and implications of large covariances between widely separated flight-time channels should be examined. Finally, engineering studies must determine a suitable method for achieving the required PRBS pulse pattern. This could be accomplished by PRBS-pulsing the ORELA trigger generator which drives the injector thyroton and accelerator klystrons. This method would probably allow the time between burst to be shorter preserving

the average ORELA power, but probably would also produce pulse intensities correlated to the PRBS sequence. ORELA also could be operated in the normal fashion with a postacceleration bending magnetic alternating the electron beam between the target-moderator and a beam dump following a PRBS. A third option is to equip one or more beam lines with mechanical PRBS choppers.

ACKNOWLEDGEMENTS

The authors gratefully acknowledge helpful discussions concerning PRBS pulsing with H. A. Mook and helpful discussion concerning ^{233}U fission cross section measurements and ORELA flux with L. W. Weston. R. Q. Wright is thanked for readily supplying the ^{233}U ENDF/B-IV fission cross section in a format suitable for our purpose. Special thanks go to M. E. Plemons for patiently typing the many drafts of this manuscript.

REFERENCES

1. M. J. Ohanian, R. B. Perez, and R. E. Uhrig, "A New Method for the Measurement of Neutron Cross-Sections," Nuclear Data for Reactors, Vol. I, International Atomic Energy Agency, Vienna, 1967, pp. 445 ff.

2. H. A. Mook, F. W. Snodgrass, and D. D. Bates, Nucl. Instr. Meth. 116 (1974) 205.

3. F. Hossfeld and R. Amadori, "Korrelationstechniken in der Flugzeitspektrometrie an Kontinuierlichen und gepulsten Quellen," internal report, Institut fur Festkorperforschung, Nuclear Research Center, Julich, Germany, May, 1972. Translated by E. G. Silver, Language Services, Knoxville, Tennessee, ORNL-tr-4646.

4. N. M. Larson, R. Crosmun, and Y. Talmi, "Theoretical Comparison of Singly Multiplexed Hadamard Transform Spectrometers and Scanning Spectrometers," Applied Optics 13 (2662), 1974. Also ORNL-TM-4603, July 1974.

5. ENDF/B-IV, Report BNL-17541 (ENDF-201), edited by D. Garber, available from the National Nuclear Data Center, Brookhaven National Laboratory, Upton, New York (October 1975).

6. D. K. Olsen, G. de Saussure, R. B. Perez, F. C. Difilippo, R. W. Ingle, and H. Weaver, "Measurement and Resonance Analysis of Neutron Transmission Through Uranium-238," Nucl. Sci. Eng. 69, 202 (1979). Also ORNL/TM-5915, October 1970.

7. E. D. Nelson and M. L. Fredman, "Hadamard Spectroscopy," J. Opt. Soc. Am. 60 (1970) 1664.

8. R. Von Jan and R. Scherm, Nucl. Instr. Meth. 80 (1970) 69.

9. D. I. Garber and R. R. Kinsey, "Neutron Cross Sections Volume II Curves," BNL325 Third Edition Volume II, January 1976.

10. L. Weston, private communication (1979).

11. J. R. Stehn, M. D. Goldberg, B. Magurno, and R. Wiener-Chasman, "Neutron Cross Sections Volume 1, Z = 1 to 20, BNL325 Second Edition Supplement No. 2, May 1964, p. 5-10-3.

APPENDIX A. EQUATIONS FOR ARBITRARY DUTY CYCLE

Throughout this report only PRBS with duty cycles of c = 1/2 have been considered. In the appendices, equations from the text are presented for arbitrary values of c; equations are numbered to identify the corresponding equations in the text. A discussion of how the optimum value of c might be chosen is also presented.

1. Theoretical Treatment Without Restriction to c = 1/2

The autocorrelation function of the PRBS $\{a_i\}$ with duty cycle c and period N is

$$C_{jk} = \sum_{i=0}^{N-1} a_{i+k}\, a_{i+j} = m[(1-c)\ \delta_{jk}+c] \tag{A1}$$

where m = 1 + c(N-1). Thus C_{jk} has the value m if j = k to within an integral multiple of N, and mc otherwise. The inverse sequence of $\{a_i\}$ is $\{a_i^*\}$ where $a_i^* = (a_i-c)/(1-c)$. Other equations from Section II are generalized and proven in Appendix B, and are not repeated here.

In the PRBS mode, the detector measures NN_b quantities $Z_k^{(n)}$, given by

$$Z_k^{(n)} = \sum_{j=0}^{N-1} \ell S_{k+jN_b}\, a_{n-j} \quad \text{for } 0 \le k < N_b,\ 0 \le n < N\ . \tag{A6}$$

This expression may be inverted to obtain the signal

$$\ell S_{k+jN_b} = \frac{1}{m} \sum_{n=0}^{N-1} Z_k^{(n)}\ a_{n-j}^*\ . \tag{A7}$$

The covariance of ℓS is given by

$$\mathrm{Cov}(\ell S_{k+jN_b},\ \ell S_{k'+j'N_b}) = \langle (\ell S_{k+jN_b} - \langle \ell S_{k+jN_b} \rangle) \times (\ell S_{k'+j'N_b} - \langle \ell S_{k'+j'N_b} \rangle) \rangle$$

where the angular brackets denote expectation value. Substituting Eq. (A7) into this expression gives

$$\mathrm{Cov}(\ell S_{k+jN_b},\ \ell S_{k'+j'N_b}) = \langle (\tfrac{1}{m})^2 \sum_{n=0}^{N-1} [Z_k^{(n)} - \langle Z_k^{(n)} \rangle]\ a^*_{n-j} \times \sum_{n'=0}^{N-1} [Z_{k'}^{(n')} - \langle Z_{k'}^{(n')} \rangle]\ a^*_{n'-j'} \rangle$$

which, because the $Z_k^{(n)}$ are independent quantities, reduces to

$$\mathrm{Cov}(\ell S_{k+jN_b},\ \ell S_{k'+j'N_b}) = \frac{1}{m^2}\ \delta_{kk'} \sum_{n=0}^{N-1} \mathrm{Var}[Z_k^{(n)}]\ a^*_{n-j}\ a^*_{n-j'} \ . \qquad \text{(A8)}$$

Because the $Z_k^{(n)}$ distribution is Poisson, the covariance becomes

$$\mathrm{Cov}(\ell S_{k+jN_b},\ \ell S_{k'+j'N_b}) = \frac{1}{m^2}\ \delta_{kk'} \sum_{n=0}^{N-1} Z_k^{(n)}\ a^*_{n-j}\ a^*_{n-j'} \ .$$

The variance for channel $k+jN_b$ follows directly from this expression, with $k = k'$ and $j = j'$:

$$\mathrm{Var}(\ell S_{k+jN_b}) = (\tfrac{1}{m})^2 \sum_{n=0}^{N-1} (a^*_{n-j})^2\ Z_k^{(n)} \ . \qquad \text{(A9)}$$

Substitution of Eq. (A6) into the expression of the covariance yields

$$\mathrm{Cov}(\ell S_{k+jN_b}, \ell S_{k'+j'N_b}) = \frac{1}{m^2}\,\delta_{kk'} \sum_{j''=0}^{N-1} \ell S_{k+j''N_b} \sum_{n=0}^{N-1} a_{n-j''}\, a^*_{n-j}\, a^*_{n-j'} ,$$

or for the variance,

$$\mathrm{Var}(\ell S_{k+jN_b}) = \left(\frac{1}{m}\right)^2 \sum_{j^\circ=0}^{N-1} \ell S_{k+j^\circ N_b} \sum_{n=0}^{N-1} a_{n-j^\circ} (a^*_{n-j})^2 . \tag{A10}$$

Using Eq. (B17) for the second sum in Eq. (A10), the variance becomes

$$\mathrm{Var}(\ell S_{k+jN_b}) = \frac{1}{m}\left(\frac{1-2c}{1-c}\,\ell S_{k+jN_b} + \frac{c}{1-c} \sum_{j^\circ=0}^{N-1} \ell S_{k+j^\circ N_b}\right) \tag{A11}$$

Note that the expression for the covariance cannot be simplified in this manner.

The relative statistical error (RSE) for the PRBS mode is given by the square root of Eq. (A11) divided by ℓS_{k+jN_b}. The ratio R of the RSE for the pseudorandom mode to the RSE for the conventional mode is

$$R_{k+jN_b} = \left[\frac{1}{m}\,\frac{NT_b}{T'_b}\left(\frac{1-2c}{1-c} + \frac{c}{1-c}\,\frac{\sum_{j^\circ=0}^{N-1} S_{k+j^\circ N_b}}{S_{k+jN_b}}\right)\right]^{1/2} . \tag{A15}$$

In the example with $S_k >> S_{k+jN_b}$ for $j \neq 0$, this ratio becomes

$$R_k \simeq \left[\frac{1}{m}\,\frac{N}{N}\left(\frac{1-2c}{1-c} + \frac{c}{1-c}\right)\right]^{1/2} = \sqrt{\frac{1}{m}} < 1 \tag{A16}$$

and, for $j \neq 0$,

$$R_{k+jN_b} \simeq \left[\frac{1}{m}\frac{N}{N}\left(\frac{1-2c}{1-c} + \frac{c}{1-c}\frac{S_k}{S_{k+jN_b}}\right)\right]^{1/2} . \tag{A17}$$

For a completely flat spectrum, where $S_{k+jN_b} \equiv S$ for all channels, the ratio is

$$R_{k+jN_b} \simeq \left[\frac{1}{m}\frac{N}{N}\left(\frac{1-2c}{1-c} + \frac{c}{1-c}\frac{NS}{S}\right)\right]^{1/2} \simeq \sqrt{\frac{1}{1-c}} > 1 . \tag{A18}$$

When time-independent background is added to the PRBS mode, the detector measures

$$Z_k^{(n)} = \ell\, d + \sum_{j=0}^{N-1} \ell S_{k+jN_b}\, a_{n-j} \tag{A20}$$

which is inverted by multiplication by $\{a^*\}$ to yield

$$\frac{\ell d}{m} + \ell S_{k+jN_b} = \frac{1}{m}\sum_{n=0}^{N-1} Z_k^{(n)}\, a^*_{n-j} \tag{A21}$$

so that the observed number of events in channel $i = k+jN_b$ is

$$O_i = \frac{\ell d}{m} + \ell S_{k+jN_b} . \tag{A22}$$

The variance of the signal is again given by Eq. (A9), with Eq. (A20) substituted for Z:

$$\mathrm{Var}\left(\frac{\ell d}{m} + \ell S_{k+jN_b}\right) = \frac{1}{m^2}\sum_{n=0}^{N-1} (a^*_{n-j})^2 \left(\ell d + \sum_{j^\circ=0}^{N-1} \ell S_{k+j^\circ N_b}\, a_{n-j}\right)$$

which reduces to

$$\mathrm{Var}\left(\frac{\ell d}{m} + \ell S_{k+jN_b}\right) = \frac{1}{m(1-c)}\left[\frac{m-c}{m}\,\ell d + (1-2c)\,\ell S_{k+jN_b} + c\sum_{j^\circ=0}^{N-1} \ell S_{k+j^\circ N_b}\right] \tag{A23}$$

2. Optimization of c

Because the variance can be taken as a figure of merit for a given PRBS configuration in the absence of uncorrelated background, the value of c which minimizes the variance can be considered optimum. Using the identity $m = cN - c + 1$ in Eq. (A11), and setting the derivative with respect to c equal to 0, gives

$$c_{opt} = \frac{1}{2S-\Sigma}\left\{S - \sqrt{\frac{1}{N-1}(\Sigma-S)\,[(N+1)\,S-\Sigma]}\right\}$$

where, to simplify the expression, we have set S_{k+jN_b} equal to S and $\sum_{j^\circ=0}^{N-1} S_{k+j^\circ N_b}$ equal to $\sum$.

Because these values depend on the particular channel under consideration, it is not possible to choose one value of c which is optimum for the entire spectrum. However, consider instead the following special cases:

(1) $S_k >> S_{k+j^\circ N_b}$ for $j^\circ \neq 0$. This is the case, for example, when no overlap occurs but the experiment is to be run simultaneously with other experiments for which PRBS is needed. Here $\sum = S$ which gives $c_{opt} = 1$, indicating that the optimum condition for this experiment is to run without PRBS at the high repetition rate.

(2) This channel contains just the average number of counts per channel; i.e. $S = \frac{1}{N} \sum$. Then $c_{opt} = 0$, indicating that the optimum condition for this channel is no PRBS and a sufficiently low repetition rate to allow no overlap. For channels with fewer counts than this, c_{opt} is either negative or complex, again indicating that PRBS has no advantage.

(3) The channel contains half of the total counts; i.e. $S = \frac{1}{2} \sum$. Here $c_{opt} = 1/2$.

Finally, consider the situation with uncorrelated background. Here the ratio of foreground to background can be taken as a figure of merit for the PRBS configuration. From Eq. (A22), that ratio is mS/d. This ratio is maximum when m is maximum, i.e. m = N - 1, corresponding to c = (N-2)/(N-1). However, for small d this choice of c improves the variance over the conventional mode only for those channels which have more counts than the sum of all overlapping channels, i.e. where $S > \sum$. Since d is small for most ORELA applications, m = N - 1 is not a useful mode for ORELA.

APPENDIX B. PROPERTIES OF PSEUDORANDOM BINARY SEQUENCES

A pseudorandom binary sequence (PRBS) with period N is an ordered set of N binary numbers (1's and 0's) whose autocorrelation function C_{jk} satisfies the condition

$$C_{jk} = \sum_{i=0}^{N-1} a_{i+k}\, a_{i+j} = m\left[(1-c)\ \delta_{jk}+c\right] \tag{B1}$$

for fixed m and c, with m an integer in the range $0 < m < N$ and c, the duty-cycle, in the range $0 \leq c \leq 1$. Delta functions and arithmetic operations on subscripts are understood to be mode N.[†] Existence and generation of these sequences are discussed in Ref. 7. Equation (B1) indicates that m of the N numbers in the PRBS are 1's, and N-m are 0's. A simple example is the case of N = 3, for which the sequence with m = 2 and c = 1/2 can be written $\{a_0, a_1, a_2\} = \{0, 1, 1\}$. From the above definition of PRBS, several important properties of these sequences may be derived.

Property 1

The duty-cycle c can be found in terms of m and N as

$$c = \frac{m-1}{N-1} . \tag{B2}$$

Proof of Property 1

From Eq. (B1) we have, setting k = 0,

$$C_{j0} = \sum_{i=0}^{N-1} a_{i+j}\, a_i = m\left[(1-c)\ \delta_{j0}+c\right] . \tag{B3}$$

[†] By $i + \ell = r \pmod N$ we mean that there is an integer s satisfying $i + \ell = sN + r$, with $0 \leq r < N$. Similarly, $\delta_{jk} \pmod N$ is 1 when $j - k = pN$ for some integer p, and 0 otherwise.

Summing over j gives

$$\sum_{j=0}^{N-1} C_{j0} = \sum_{i=0}^{N-1} a_i \left(\sum_{j=0}^{N-1} a_{i+j} \right) \tag{B4}$$

$$= m(1-c) \sum_{j=0}^{N-1} \delta_{j0} + mc \sum_{j=0}^{N-1} 1 = m(1-c) + mcN = m + (N-1)mc \ . \tag{B5}$$

If we set k = j in Eq. (B1), we find $C_{jj} = \sum_{i=0}^{N-1} a_{i+j}^2 = m$. Because the a_{i+j} are either 0 or 1, $a_{i+j} \equiv a_{i+j}^2$; consequently, this equation may be written

$$\sum_{i=0}^{N-1} a_{i+j} = m \ . \tag{B6}$$

Substitution of this value for the expression in parenthesis in Eq. (B4) gives

$$\sum_{j=0}^{N-1} C_{j0} = \left(\sum_{i=0}^{N-1} a_i \right) m = m + (N-1)mc \tag{B7}$$

or, again using Eq. (B6) for the quantity in parenthesis,

$$m^2 = m + (N-1)mc \tag{B8}$$

which reduces to

$$c = \frac{m-1}{N-1} \ . \tag{B9}$$

Property 2

Define the inverse sequence $\{a_i^*\}$ by

$$a_i^* = \frac{a_i - c}{1-c} \quad . \tag{B10}$$

Then the cross-correlation of $\{a_i^*\}$ with $\{a_i\}$ yields

$$\sum_{i=0}^{N-1} a_{i+j}^* \, a_{i+k} = m \, \delta_{jk}^{\text{mod } N} \quad . \tag{B11}$$

In our example, $\{a_0^*, a_1^*, a_2^*\} = \{-1, 1, 1\}$ so that

$$\sum_{i=0}^{2} a_{i+j}^* \, a_{i+k} = (0+1+1) = 2 \text{ for } j=k$$

$$= (0+1-1) = 0 \text{ for } j \neq k \quad .$$

Proof of Property 2

The proof follows directly from the definitions:

$$\sum_{i=0}^{N-1} \frac{a_{i+j} - c}{1-c} \, a_{i+k} = \frac{1}{1-c} \sum_{i=0}^{N-1} a_{i+j} \, a_{i+k} - \frac{c}{1-c} \sum_{i=0}^{N-1} a_{i+k}$$

$$= \frac{1}{1-c}\left[m(1-c) \, \delta_{jk}^{\text{mod } N} + mc - cm\right] \quad . \tag{B12}$$

Property 3

The summation over all terms in the inverse sequence $\{a_i^*\}$ gives

$$\sum_{i=0}^{N-1} a_i^* = 1 \quad . \tag{B13}$$

In our example $a_0^* + a_1^* + a_2^* = -1 + 1 + 1 = 1$.

Proof of Property 3

The proof follows directly from the definition of a_i^*, and from Eqs. (B2) and (B6):

$$\sum_{i=0}^{N-1} a_i^* = \frac{1}{1-c} \sum_{i=0}^{N-1} (a_i - c) = \frac{1}{1-c}(m - cN) = 1 \ . \tag{B14}$$

Property 4

The summation over the square of the terms in the symmetrized sequence gives

$$\sum_{i=0}^{N-1} (a_i^*)^2 = \frac{m-c}{1-c} \ . \tag{B15}$$

In our example $a_0^{*2} + a_1^{*2} + a_2^{*2} = 3$, and $\frac{m-c}{1-c} = \frac{2-1/2}{1-1/2} = 3$.

Proof of Property 4

Again the proof follows directly from the definition of a_i^*, using Eqs. (B1), (B2), and (B6)

$$\sum_i (a_i^*)^2 = \left(\frac{1}{1-c}\right)^2 \sum_{i=0}^{N-1} (a_i - c)^2 = \left(\frac{1}{1-c}\right)^2 \sum_{i=0}^{N-1} (a_i^2 - 2a_i c + c^2)$$

$$= \left(\frac{1}{1-c}\right)^2 (m - 2cm + c^2 N) = \frac{m-c}{1-c} \ . \tag{B16}$$

Property 5

This property is required for evaluation of the variance [see Eq. (A8)] :

$$\sum_{n=0}^{N-1} a_{n-i} (a_{n-j}^*)^2 = \frac{m}{1-c} \left[(1-2c)\ \delta_{ij} + c\right] \tag{B17}$$

In our example $0 + 1 + 1 = \frac{2}{1/2}[1/2] = 2$.

Proof of Property 5

The proof follows from the definition of a_i^*, using Eqs. (B1) and (B11), and noting that $a_{n-j}\, a^*_{n-j} = a_{n-j}$:

$$\sum_{n=0}^{N-1} a_{n-i}\, \frac{a_{n-j}-c}{1-c}\, a^*_{n-j} = \frac{1}{1-c} \sum_{n=0}^{N-1} a_{n-i}\, a_{n-j}\, a^*_{n-j} - \frac{c}{1-c} \sum_{n=0}^{N-1} a_{n-i}\, a^*_{n-j}$$

$$= \frac{1}{1-c}\left[m(1-c)\, \delta_{ij} + mc\right] - \frac{c}{1-c}\, m\, \delta_{ij}$$

$$= \frac{m}{1-c}\left[(1-2c)\, \delta_{ij} + c\right] . \qquad \text{(B18)}$$

Property 6

If N' is any integer which has no common divisors with N, then

$$\sum_{i=0}^{N-1} a_{iN'+j}\, a_{iN'+k} \equiv C_{jk} , \qquad \text{(B19)}$$

since iN' (mod N) covers the entire range of values from 0 to N - 1. In our example with N = 3, take N' = 5. Then i = 0 gives iN' = 0, i = 1 gives iN' = 5(mod 3) = 2, and i = 2 gives iN' = 10(mod 3) = 1.

Proof of Property 6

Set p = iN'. As i varies from 0 to N - 1, p also spans the entire range of i from 0 to N - 1 (though not necessarily in order). Suppose this were not so; i.e., suppose for $i \neq i'$ we had (iN' = i'N') (mod N). Without loss of generality, take i > i'. This would mean that there are integers q, r, and s with $0 \leq q < N$, such that iN' = q + rN and i'N' = q + sN. Subtracting these two equations gives (i-i') N' = (r-s) N.

Since N and N' have no common divisors, this equation requires that $i - i' = tN$ (and $r - s = tN'$) where t is some integer ≥ 1, which cannot be true since $N > i \geq i' \geq 0$.

Therefore, the summation in Eq. (B17) may be written $\sum_{p=0}^{N-1} a_{p+j}\, a_{p+k}$ which is exactly C_{jk}.

Property 7

If $\{a_i\}$ is a PRBS of period N and duty cycle c, and $\{b_i\}$ is a PRBS of period N' and duty cycle c', and N and N' have no common divisors, then

$$\sum_{i=0}^{L-1} a_{i+\alpha}\, a_{i+\beta}\, b_{i+\gamma}\, b_{i+\varepsilon}$$

$$= m\left[(1-c)\ \delta_{\alpha\beta}^{\text{mod } N} + c\right] m' \left[(1-c')\ \delta_{\gamma\varepsilon}^{\text{mod } N'} + c'\right] \qquad \text{(B20)}$$

where $L = N\,N'$, $m = 1 + c(N-1)$, and $m' = 1 + c'(N'-1)$.

Proof of Property 7

Replace i by $kN' + j$, and $\sum_{i=0}^{L-1}$ by $\sum_{j=0}^{N'-1} \sum_{k=0}^{N-1}$. Note that $b_{kN'+j+\gamma} \equiv b_{j+\gamma}$. Then Eq. (B20) can be written

$$\sum_{j=0}^{N'-1} b_{j+\gamma}\, b_{j+\delta}\left(\sum_{k=0}^{N-1} a_{kN'+j+\alpha}\, a_{kN'+j+\beta}\right). \qquad \text{(B21)}$$

By property 4, the quantity in parenthesis is equivalent to $\sum_{n=0}^{N-1} a_{n+\alpha}\, a_{n+\beta}$ and both sums in (B21) are of the form (B1).

APPENDIX C. OTHER APPLICATIONS OF PRBS PULSING AT ORELA

Assuming that pseudorandom pulsing of ORELA can be achieved by means of a mechanical chopper placed in the beam line, at least two other applications suggest themselves. The first is a method of increasing resolution without shortening pulse width. The second is a method of performing double time-of-flight experiments with a single detector. The theory behind both applications is presented here without comment on the ease or difficulty of implementing such procedures and without comparison of these procedures to others which might accomplish the same objectives.

1. Increasing Resolution

Consider an arbitrary location along the beam line between the source and the detector. At this location the burst has spread in time as shown in Fig. 16. A PRBS chopper of period N inserted at this point can be used to increase time resolution by dividing this time spread into M channels of width θ, with $M \leq N$.

If a neutron of energy E_i requires time t_i to travel from chopper to detector, the number of counts recorded by the detector is

$$Z_k^{(n)} = \ell \sum_{j=0}^{M-1} \sum_{i=0}^{N_b-1} R_i \, \phi_{ij} \, \delta(t_i+j\theta, t_k) \, a_{nN_b+j} \qquad (C1)$$

where ϕ_{ij} is the flux of particles of energy E_i reaching the chopper at time $j\theta$ and R_i is the sample response to neutrons of energy E_i (R_i is in fact the quantity of physical interest). All times are given relative to the time at which the fastest neutron reaches the chopper. The PRBS member a_{nN_b} represents the state of the chopper at this reference time;

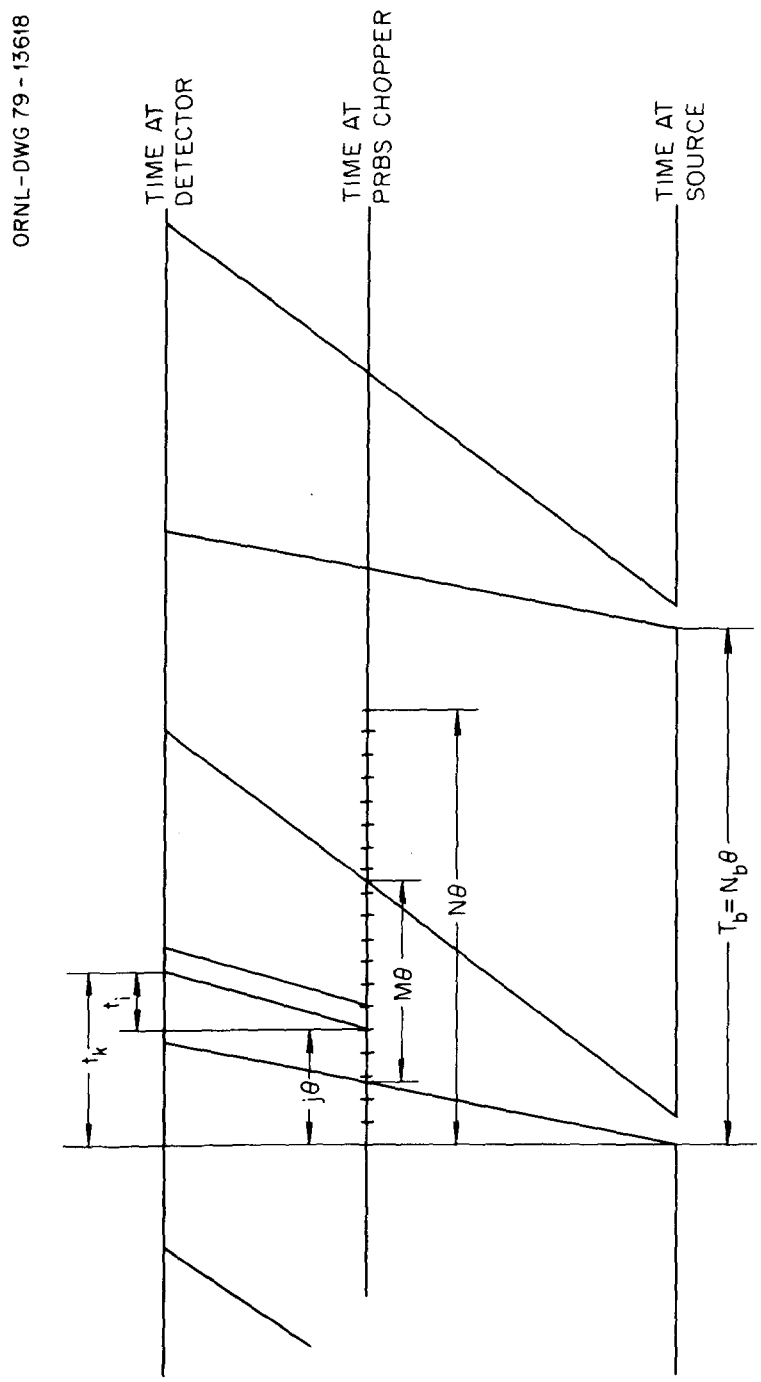

Fig. 16. Time sequence for neutron production and detection with a mechanical PRBS chopper inserted into the beam line. Resolution is thereby increased because the time at which the neutron leaves the source is more precisely determined.

$a_{nN_b + j}$ represents the state of the chopper at time $j\theta$. The factor ℓ in Eq. (C1) is the number of times the experiment is repeated, i.e. the number of bursts divided by N.

If channel widths at source and detector are equal to channel widths at the chopper, Eq. (C1) becomes

$$Z_k^{(n)} = \ell \sum_{i=0}^{N_b-1} R_i \, \phi_{i,k-i} \, a_{nN_b+k-i} \tag{C2}$$

where k labels the time between bursts, $0 \leq k < N_b$, and n labels the particular burst or, equivalently, the state of the chopper in the PRBS sequence at the reference time, with $0 \leq n < N$. In order for the NN_b quantities $Z_k^{(n)}$ to be unique, it is necessary that N and N_b have no common divisors; otherwise $\{a_{nN_b}\}$ would not span the entire set $\{a_i\}$.

To extract the sample response from Eq. (C2), multiply by the inverse sequence $\{a_{nN_b+k-j}\}$:

$$\ell R_j \, \phi_{j,k-j} = \frac{1}{m} \sum_{n=0}^{N-1} Z_k^{(n)} \, a^*_{nN_b+k-j} \, . \tag{C3}$$

This expression can then be summed over k to give a result dependent only on energy and independent of detector time

$$\ell R_j \, \Phi_j = \frac{1}{m} \sum_{n=0}^{N-1} \sum_{k=j}^{M+j-1} Z_k^{(n)} \, a^*_{nN_b+k-j} \, . \tag{C4}$$

Here Φ_j is the sum of the flux of neutrons of energy E_j reaching the chopper at all times, that is

$$\Phi_j = \sum_{k=j}^{M+j-1} \phi_{j,k-j} = \sum_{k=0}^{M-1} \phi_{j,k} \quad . \tag{C5}$$

Limits on the sums over k in Eqs. (C4) and (C5) explicitly express the restriction that $\phi_{j,k} = 0$ for $k \geq M$.

From Eq. (C4) the variance can be shown to be

$$\mathrm{Var}(\ell R_j \; \Phi_j) = \frac{1}{m^2} \sum_{n=0}^{N-1} \sum_{k=j}^{M+j-1} Z_k^{(n)} (a^*_{nN_b+k-j})^2 \quad . \tag{C6}$$

Equations (C4) and (C6) can be used to evaluate the sample response R_j and the variance, once the flux Φ_j is established to sufficient accuracy. This flux can be measured by removing the sample from the beam line and recording

$$Y_k^{(n)} = \ell' \sum_{i=0}^{N_b-1} \phi_{i,k-i} \; a_{nN_b+k-i} \quad . \tag{C7}$$

Multiplication by the inverse sequence gives

$$\ell' \phi_{j,k-j} = \frac{1}{m} \sum_{n=0}^{N-1} Y_k^{(n)} \; a^*_{nN_b+k-j} \tag{C8}$$

which in turn can be summed over k to give

$$\ell' \Phi_j = \frac{1}{m} \sum_{n=0}^{N-1} \sum_{k=j}^{M+j-1} Y_k^{(n)} \; a^*_{nN_b+k-j} \tag{C9}$$

with variance

$$\mathrm{Var}(\ell' \Phi_j) = \frac{1}{m^2} \sum_{n=0}^{N-1} \sum_{k=j}^{M+j-1} Y_k^{(n)} (a^*_{nN_b+k-j})^2 \quad . \tag{C10}$$

2. Double Time of Flight

In order to measure both incoming and outgoing energies for a neutron impinging on a sample, we introduce a PRBS chopper of period N at the location of the sample, as shown in Fig. 17. Let S_{ij} represent the signal for neutrons of incident energy E_i and outgoing energy E_j; t_i represents the travel time from source to sample and t_j the travel time from sample to detector. At time t_k for the n^{th} burst the detector records $Z_k^{(n)}$ counts,

$$Z_k^{(n)} = \sum_{i=0}^{N_b-1} \sum_{j=0}^{N_b-1} \ell S_{ij}\, a_{nN_b+i}\, \delta(t_i+t_j-t_k) \tag{C11}$$

where there are N_b time channels between bursts, and a_{nN_b} represents the state of the PRBS at the time of the n^{th} burst. The factor ℓ indicates the number of times the experiment is repeated; here ℓ is the number of bursts divided by N. If channel widths at the chopper are equal to those at the source and detector, Eq. (C11) reduces to

$$Z_k^{(n)} = \sum_{i=0}^{k} \ell S_{i,k-i}\, a_{nN_b+i} \ . \tag{C12}$$

Here the implicit restriction $S_{ij} = 0$ for $j < 0$ has been made explicit by choice of the limits on the summation.

If N and N_b have no common divisors, Eq. (C12) may be multiplied by the inverse function $\{a^*_{nN_b+r}\}$ to yield

$$\sum_{i=0}^{k} \ell S_{i,k-i}\, \delta_{ir}^{\text{mod } N} = \frac{1}{m} \sum_{n=0}^{N-1} Z_k^{(n)}\, a^*_{nN_b+r} \ . \tag{C13}$$

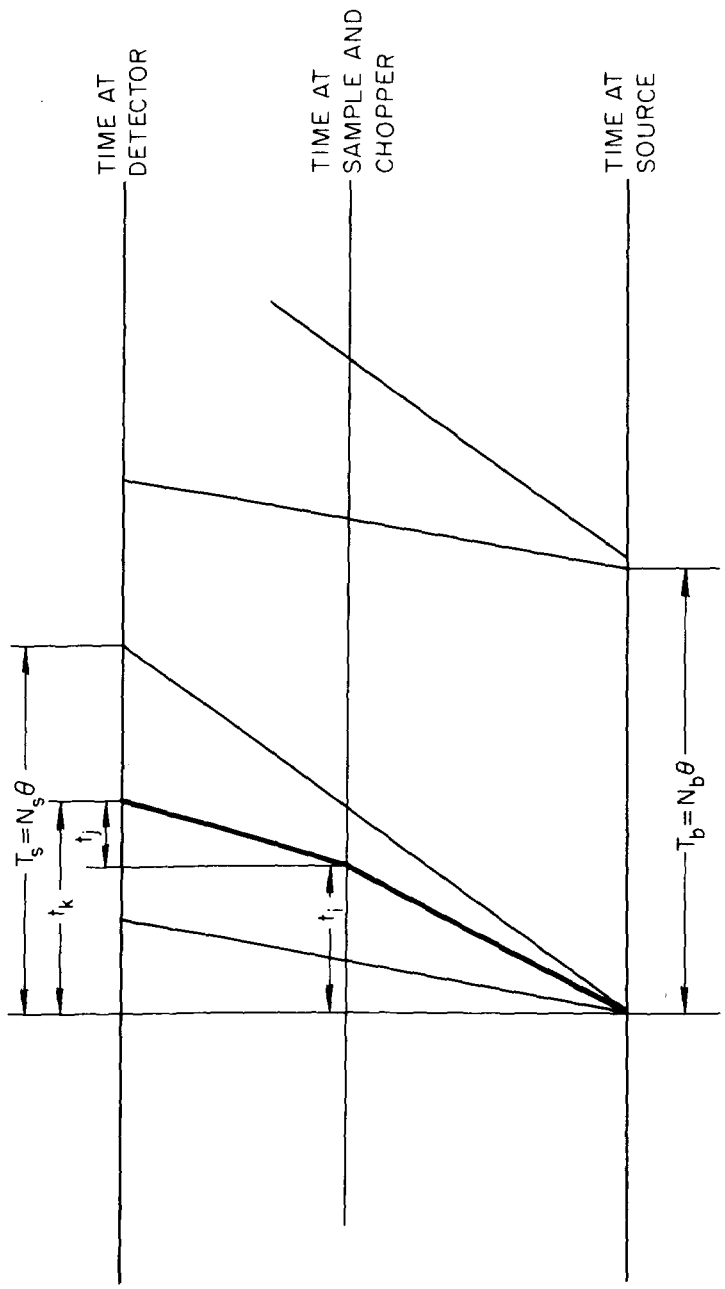

Fig. 17. Time sequence for neutron production and detection in a double-time-of-flight experiment, with a mechanical PRBS chopper inserted into the beam line at the position of the chopper. Use of the PRBS chopper allows measurement of both incoming and outgoing neutron TOF's simultaneously.

The right-hand side of this expression will always be equal to $S_{r,k-r}$ only if the ranges of i and r are properly restricted, that is only if i and r cannot be greater than N. The range of i is $0 \leq i < N_s \leq N_b$, where N_s is the number of channels i for which nonzero signals S_{ij} occur. The range of r is $0 \leq r < N$, since larger values of r would be redundant (that is, $a_{nN_b+r+N} = a_{nN_b+r}$). Therefore N must be chosen greater than N_s in order to give

$$\ell S_{r,k-r} = \frac{1}{m} \sum_{n=0}^{N-1} Z_k^{(n)} \, a^*_{nN_b+r} \, . \tag{C14}$$

The variance for this signal is

$$\mathrm{Var}(\ell S_{r,k-r}) = \frac{1}{m^2} \sum_{n=0}^{N-1} (a^*_{nN_b+r})^2 \, Z_k^{(n)} \tag{C15}$$

which can be written in terms of S_{ij} as

$$\mathrm{Var}(\ell S_{r,k-r}) = \frac{1}{m^2} \sum_{i=0}^{k} \ell S_{i,k-i} \sum_{n=0}^{N-1} a_{nN_b+i} (a^*_{nN_b+r})^2 \, . \tag{C16}$$

ORNL/TM-6632
ENDF-290
Dist. Category UC-79d

INTERNAL DISTRIBUTION

1-2. L. S. Abbott
3. Z. W. Bell
4. J. S. Crowell
5. H. Goldstein
6. R. Gwin
7. D. C. Larson
8-27. N. M. Larson
28. F. C. Maienschein
29. G. S. McNeilly
30-39. D. K. Olsen
40. R. W. Peelle
41. F. G. Perey
42. R. R. Spencer
43. H. A. Todd
44. J. H. Todd
45. L. W. Weston
46. P. Greebler (consultant)
47. W. B. Loewenstein (consultant)
48. R. Wilson
49-50. Central Research Library
51. ORNL Y-12 Technical Library
Document Reference Section
52-53. Laboratory Records Dept.
54. ORNL Patent Office
55. Laboratory Records (RC)

EXTERNAL DISTRIBUTION

56. Office of Assistant Manager, Energy Research and Development, DOE-ORO, Oak Ridge, Tennessee 37830
57-58. DOE Division of Reactor Research and Development, Washington, D.C. 20545: Director
59-299. For distribution as shown in TID-4500 Distribution Category UC-79d, Liquid Metal Fast Breeder Reactor Physics - Base (60 copies - ENDF distribution)

UNITED STATES DEPARTMENT OF ENERGY
P.O. BOX 62
OAK RIDGE, TENNESSEE 37830

OFFICIAL BUSINESS
PENALTY FOR PRIVATE USE, $300

POSTAGE AND FEES PAID
UNITED STATES
DEPARTMENT OF ENERGY

U.S.MAIL

Brookhaven National Laboratory ENDF
ATTN: Dr. Charles L. Dunford
National Nuclear Data Center
Building 197
Upton, NY 11973

PRINTED MATTER – BOOKS